AD-A061 063 BOEING AEROSPACE CO HUNTSVILLE AL. ARMY SYSTEMS DIV F/G 19/7
ROCKET MOTOR PEAK NOISE REDUCTION PROGRAM.(U)
SEP 78 C R CARTER
UNCLASSIFIED D256-10514 DRDMI-T-CR-78-27 DAAK40-78-C-0038 NL

END
DATE FILMED
-79
DDC

(2) LEVEL II

REPORT T-CR-78-27

ROCKET MOTOR PEAK NOISE REDUCTION PROGRAM

CHARLES R. CARTER

BOEING AEROSPACE COMPANY
ARMY SYSTEMS DIVISION
220 WYNN DRIVE
HUNTSVILLE, AL 35807

30 SEPTEMBER 1978

FINAL REPORT

APPROVED FOR PUBLIC RELEASE; DISTRIBUTION UNLIMITED

PREPARED FOR:

TECHNOLOGY LABORATORY
PROPULSION DIRECTORATE
US ARMY MISSILE RESEARCH AND DEVELOPMENT COMMAND
REDSTONE ARSENAL, AL 35809

DISPOSITION INSTRUCTIONS

Destroy this report when it is no longer needed.
Do not return it to the originator.

DISCLAIMER

The findings in this report are not to be construed as an official Department of the Army position unless so designated by other authorized documents.

TRADE NAMES

Use of trade names or manufacturer in this report does not constitute an official endorsement or approval of the use of such commercial hardware or software.

UNCLASSIFIED

SECURITY CLASSIFICATION OF THIS PAGE *(When Data Entered)*

REPORT DOCUMENTATION PAGE

READ INSTRUCTIONS BEFORE COMPLETING FORM

1. REPORT NUMBER: T-CR-78-27
2. GOVT ACCESSION NO.:
3. RECIPIENT'S CATALOG NUMBER: rept.
4. TITLE *(and Subtitle)*: Rocket Motor Peak Noise Reduction Program.
5. TYPE OF REPORT & PERIOD COVERED: Final 1 Jan [illegible] through 30 Sep 78
6. PERFORMING ORG. REPORT NUMBER: D256-10514
7. AUTHOR(s): Charles R. Carter
8. CONTRACT OR GRANT NUMBER(s): DAAK40-78-C-0038
9. PERFORMING ORGANIZATION NAME AND ADDRESS:
Boeing Aerospace Company
Army Systems Division
220 Wynn Drive
Huntsville, AL 35807
10. PROGRAM ELEMENT, PROJECT, TASK AREA & WORK UNIT NUMBERS:
11. CONTROLLING OFFICE NAME AND ADDRESS: DRDMI-T
12. REPORT DATE: 30 September 1978
13. NUMBER OF PAGES: 95
14. MONITORING AGENCY NAME & ADDRESS *(if different from Controlling Office)*:
Technology Laboratory
Propulsion Directorate
US Army Missile Research and Development Command
Redstone Arsenal, AL 35809
15. SECURITY CLASS. *(of this report)*: UNCLASSIFIED
15a. DECLASSIFICATION/DOWNGRADING SCHEDULE:
16. DISTRIBUTION STATEMENT *(of this Report)*:
Approved for public release; distribution unlimited
87 p.
17. DISTRIBUTION STATEMENT *(of the abstract entered in Block 20, if different from Report)*:
18. SUPPLEMENTARY NOTES:
19. KEY WORDS *(Continue on reverse side if necessary and identify by block number)*:
Peak Noise
Suppressor
20. ABSTRACT *(Continue on reverse side if necessary and identify by block number)*:

This report describes the design, test and analysis of two techniques being developed for reducing the peak noise produced by a shoulder-fired rocket weapon system. The tests have verified that the peak noise produced by the M-72 rocket motor can be reduced at the gunner's position by 10 db with a baffled cylinder suppressor and by 1.3 db by aerodynamically shaping the nozzle closure. Analysis of the unsuppressed and suppressed peak noise generated by the M-72 rocket motor indicate that the peak noise in the near field is

DD FORM 1 JAN 73 1473 EDITION OF 1 NOV 65 IS OBSOLETE

UNCLASSIFIED

SECURITY CLASSIFICATION OF THIS PAGE *(When Data Entered)*

410 935

LB

20. (Continued)

produced by the energy associated with a strong pressure wave that can be correlated with spherically symmetric point explosion data. The hardware test data base and analysis techniques developed have provided a basis for the design of prototype field weight suppressor systems for protecting the gunner and crew from the intense peak noise produced by both man-portable and shoulder-fired rocket weapon systems.

THE BOEING COMPANY

CODE IDENT. NO. 81205

THIS DOCUMENT IS:

CONTROLLED BY 2-8101

ALL REVISIONS TO THIS DOCUMENT SHALL BE APPROVED BY THE ABOVE ORGANIZATION PRIOR TO RELEASE.

PREPARED UNDER ☒ CONTRACT NO. DAAK40-78-C-0038

☐ IR&D

☐ OTHER

DOCUMENT NO. D256-10514 MODEL

TITLE ROCKET MOTOR PEAK NOISE REDUCTION PROGRAM

ORIGINAL RELEASE DATE September 30, 1978

ISSUE NO. TO

ADDITIONAL LIMITATIONS IMPOSED ON THIS DOCUMENT WILL BE FOUND ON A SEPARATE LIMITATIONS PAGE

PREPARED BY C. R. Carter

SUPERVISED BY L. B. McTigue

APPROVED BY Larry B. McTigue

TABLE OF CONTENTS

LIST OF ILLUSTRATIONS

LIST OF ILLUSTRATIONS (Continued)

LIST OF ILLUSTRATIONS (Continued)

LIST OF TABLES

ACKNOWLEDGEMENTS

Contributions to the hardware design, test area preparations, test fixture setup, motor loading, instrumentation setup, raw data interpreation, data analysis and document preparation were made by the following personnel:

Boeing Aerospace Company

Charles Carter
Patty Dorsett
Billy Garrison
Alex Hunter
Harry Kindred
George Pinson
Diana Sisson

ERC, Inc.

Dr. F. G. Collins
Dr. M. Kurosaka
Dr. J. R. Maus
Dr. A. Vakili
Dr. J. M. Wu

MIRADCOM Propulsion Directorate

Jerry Arszman
Charles Bishop
Don Ifshin
Chester Norman
Buddy Ratliff
Bob Sawada
John Tate
Paul Williams
Billy Wright

Any questions concerning the data and analyses should be directed to the author:

Charles R. Carter
205-837-4348

REFERENCES

1. D256-10221, Small Rocket Sound Reduction, January 10, 1971.

2. Sedov, L. I., Similarity and Dimensional Methods in Mechanics, Academic Press, 1959.

3. Glass, I. I., Shock Waves and Man, The University of Toronto Press, 1974.

4. Thompson, P. A., Compressible Fluid Dynamics, McGraw-Hill, 1971.

5. Baker, W. E., Explosions in Air, University of Texas Press, 1973.

6. Whitham, G. B., Linear and Nonlinear Waves, John Wiley and Sons, 1973.

1.0 INTRODUCTION AND SUMMARY

The intense noise peak generated during launch of a shoulder-fired rocket can be reduced significantly by baffled sound suppressors. Suppressor hardware were developed and hot-fired behind the M-72 rocket motor. Noise reductions up to 10 db were achieved in a series of 45 hot-firings conducted by MIRADCOM.

Theoretical prediction models were developed and improved via correlation with test results. These models correlate well with the test data and provide a basis for improving the sound suppressor design.

This document presents the results of both the experimental and theoretical development. It is concluded that the program has:

1. Demonstrated the effectiveness of the baffled sound suppressor design.
2. Identified promising advanced concepts for future test and evaluation.
3. Provided an experimental data base and theoretical tools to support development of a field-weight prototype system.

The remainder of the Introduction and Summary describes the mechanisms producing the peak noise, and summarizes test and analytical results.

Design goals for man-portable and shoulder-fired rocket systems have been directed towards achieving maximum range, accuracy and lethality while minimizing cost and weight. The local noise level generated by firing high performance rocket systems is close to the maximum noise level that the crew can withstand even with ear protection. The high noise level produced by these weapon systems not only presents a potential physical hazard to the user but also acts as a technological barrier to development of future high performance rocket systems. The schematic of a typical shoulder fired rocket launch, shown in Figure 1-1, illustrates the local

1.0 (Continued)

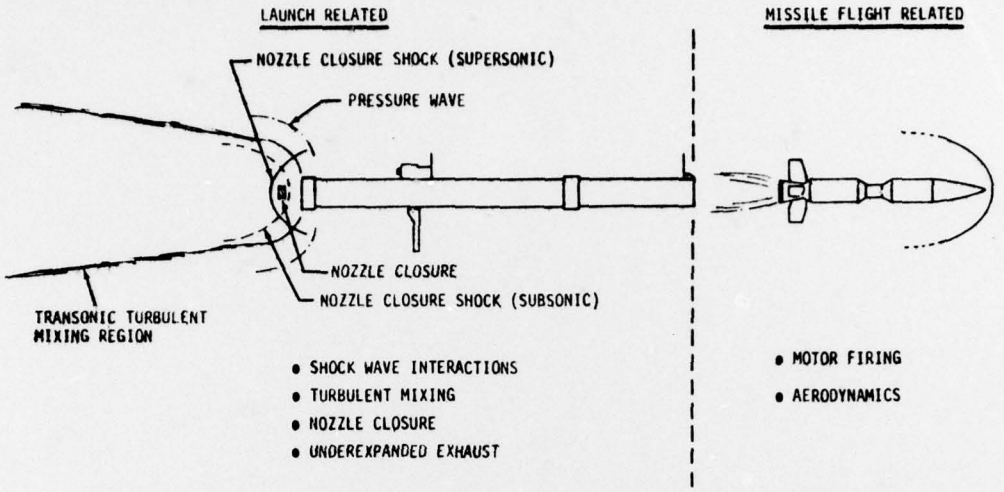

FIGURE 1-1. PRIMARY LAUNCH AND MISSILE FLIGHT RELATED NOISE SOURCES

noise sources generated by the weapon. After motor ignition, the motor chamber pressure expells the nozzle closure at a high speed. A shock wave is generated for a short distance as the closure moves away from the motor nozzle. This shock either preceeds or trails the closure depending on the closure velocity when compared to the exhausting gas velocity. A second pressure wave is caused by the high velocity gasses leaving the nozzle with the closure. The peak noise is of a transient nature; thus it is a function of time and location. It is caused primarily by the exhaust gasses expanding into the atmosphere, and secondly by nozzle closure motion. The peak noise pressure wave is followed by a brief "steady state" gas flow and reflected noise from the ground and local objects as well as noise generated at the forward end of the launcher. These effects produce noise much lower than the transient burst and do not drive suppressor design.

The Boeing Army Systems Division began a noise suppressor research program in 1976. A subscale hardware development and test program demonstrated that the peak noise produced by the pressure wave could be reduced by at

1.0 (Continued)

least 10 db with a baffled suppressor mounted to the launcher aft of the motor. Based on this subscale test data, suppressor hardware was designed for the M-72 weapon system and a joint MIRADCOM/Boeing test series was conducted in 1978. These tests were designed to verify that the suppressor concepts would work on full scale hardware and to establish an experimental/theoretical data base for extending the design to an actual field weight system.

The M-72 noise suppressing hardware, that was designed and tested, addressed both possible sources of the peak noise. The nozzle closure shock strength was varied by changing the aerodynamic shape of the closure on both the forward and aft ends and by varying the pressure required to expel the closure. The pressure wave generated by the expanding exhaust gas was contained in several configurations of baffled suppressors. The peak noise reduction capability of each hardware configuration was determined and the data were analyzed to determine theoretical relationships that can be used to predict the performance of similar hardware when used on other rocket systems.

When the baffled suppressors of the type shown in Figure 1-2 were attached

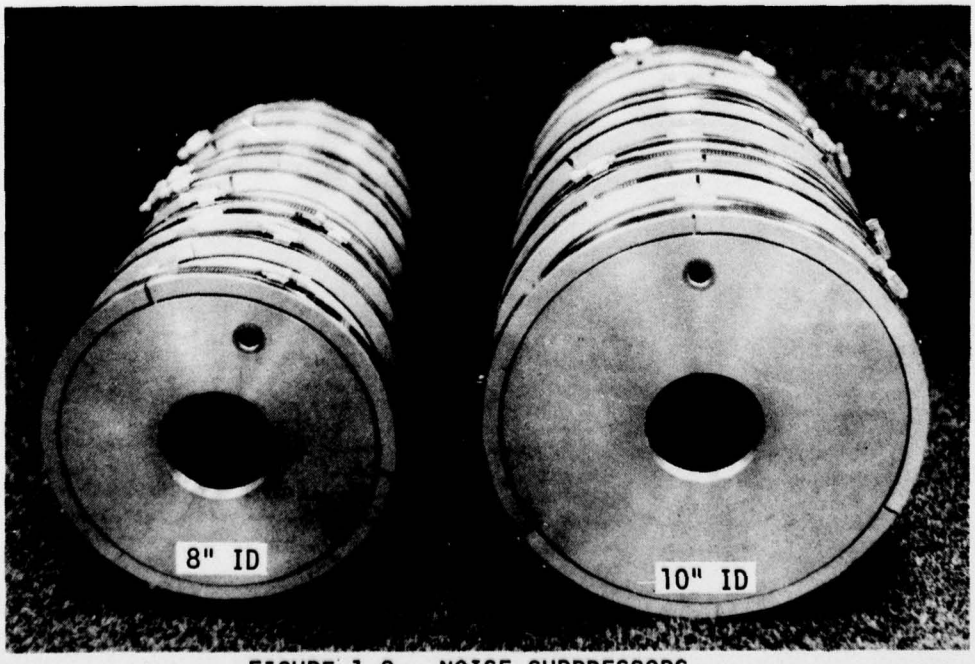

FIGURE 1-2. NOISE SUPPRESSORS

1.0 (Continued)

to the launcher aft of the motor, the peak noise at the gunners position was reduced from 169.7 db to 159.1 db. The performance and pressure data obtained with these "boilerplate" suppressor designs have shown that these suppressors can be redesigned to field weight systems that have equal or better performance.

The test results of the aerodynamically shapped nozzle closures have shown that the ogive/blunt closure configuration shown in Figure 1-3 can reduce

STANDARD M-72 OGIVE/BLUNT

FIGURE 1-3. NOZZLE CLOSURES

the peak noise at the gunners position by 1.3 db when compared to the standard M-72 nozzle closure.

An empirical method has been developed to estimate the energy in the pressure wave by integrating the initial pressure pulse measured when the wave passes the sound pressure level instrumentation. The estimated energy was correlated with the non-dimensional distance from the source and the results are shown in Figure 1-4. These data were found to correlate well with the spherically symmetric point explosion data. As can be seen from the energy data presented in Figure 1-4, the suppressor is not just acting as a noise shield but is substantially reducing the acoustic energy when compared to the unsuppressed data.

1.0 (Continued)

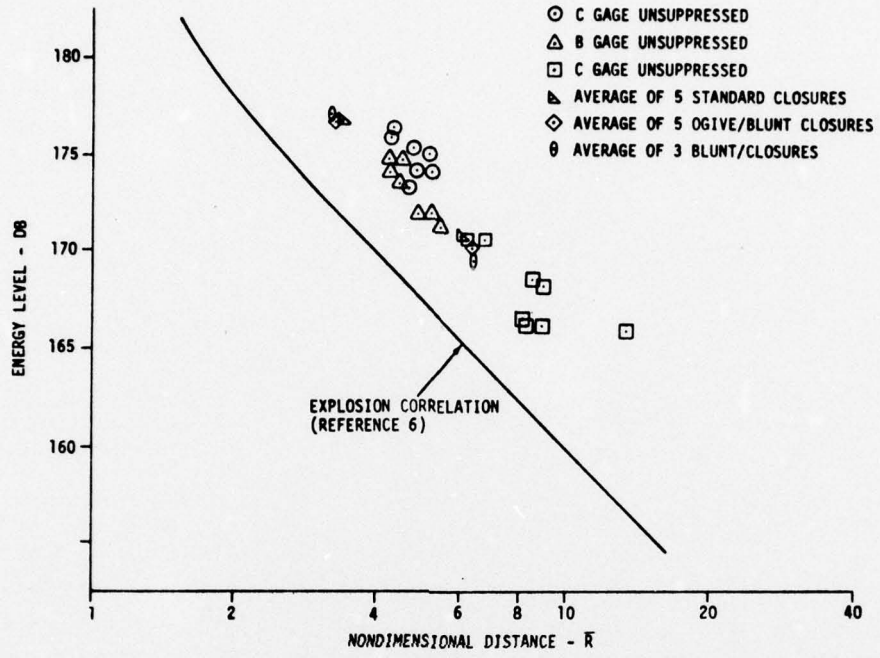

FIGURE 1-4. CORRELATION OF ENERGY DATA WITH EXPLOSION THEORY

The theory of shock propagation through a non-uniform duct has been applied to the baffle concept used in the suppressor design. This theoretical method was used to obtain the reduction in pressure wave strength as it passes through a series of baffles. The reduction in pressure wave strength for the analytical suppressor was calculated to be between 7 and 13 db compared to 8.3 db obtained in the suppressor tests.

Based on the test data, the physical explanation of the noise attenuation through baffles and the analytical results obtained, noise suppressor configurations can be developed that have up to 12 db noise reduction capability. These suppressors must have a solid case to shield the gunner, several baffles (at least three) and should have a divergent cross-section shape. If the additional shielding effect of the exhaust gas stream is utilized, the suppressor concept would have a configuration as shown in Figure 1-5.

1.0 (Continued)

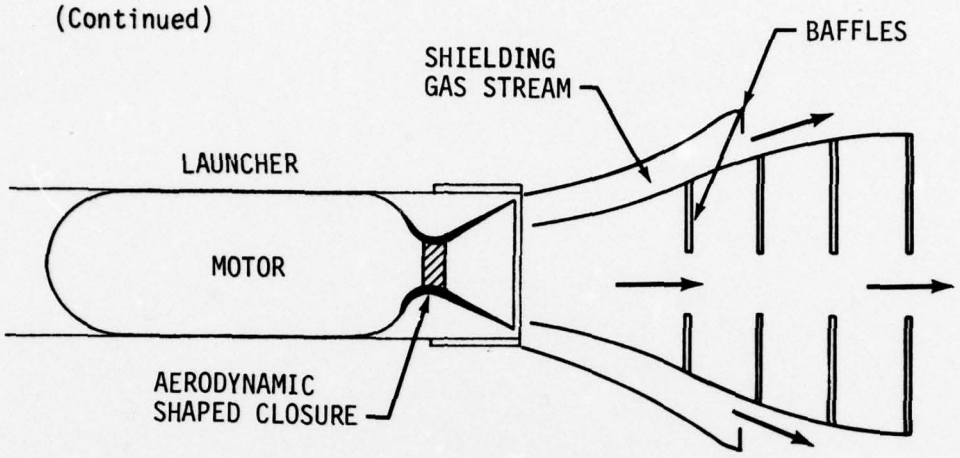

FIGURE 1-5. ADVANCED SUPPRESSOR CONCEPT

These tests and analytical results have confirmed that the energy which produces the peak noise is contained in a pressure wave that is emitted when the nozzle closure is expelled from the motor. A second advanced suppressor concept that confines this pressure wave and nozzle closure could take the form of a bag attached to the launcher as shown in Figure 1-6.

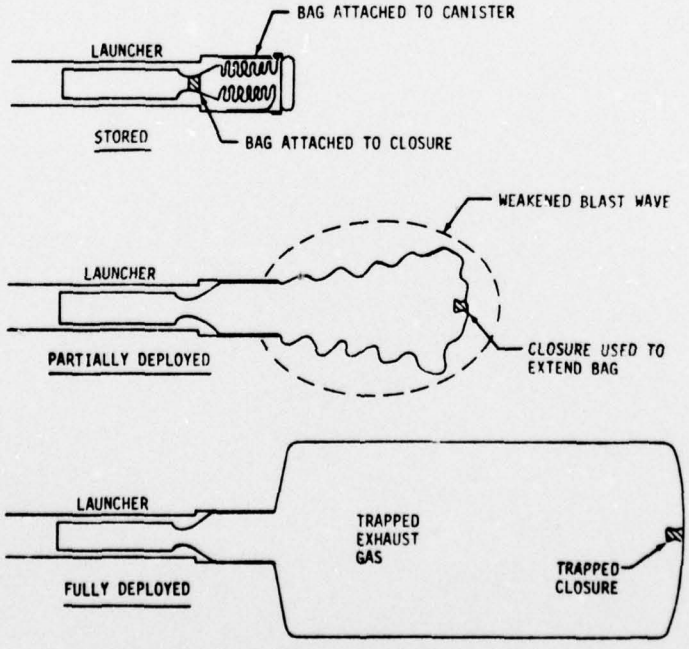

FIGURE 1-6. ENERGY ABSORBING MATERIAL BAG

1.0 (Continued)

It is estimated that a fielded system of this design would weigh less than 3 lbs., and could be folded to fit within a small cannister at the rear of the launch tube. In addition to reducing noise, this design also reduces flash and smoke signature. The bag material would have to be an energy absorbing porous reinforced foam that would attenuate the pressure wave energy as it passes through. Such a bag has been tested during the Boeing Research Program and produced over 11 db reduction at the gunners position when compared to the unsuppressed case.

The following paragraphs describe the noise suppressor hardware design, test and analyses tasks that were performed as part of the Rocket Motor Peak Noise Reduction Program.

2.0 NOISE SUPPRESSING NOZZLE CLOSURE DESIGN AND EVALUATION

This part of the Peak Noise Reduction Program was performed to understand the noise generated by the explusion of the nozzle closure during the firing of a small rocket motor. As can be seen from Figure 2-1, there are several postulations available about how the noise is generated when a rocket motor is fired. At some pressure level the nozzle closure is expelled from the nozzle at a high velocity. A shock wave will be formed around the nozzle closure generated by its own motion (if supersonic), or by the supersonic flow of hot gasses impinging on the closure. In either case, the shock wave produced is interpreted by the gunner as a noise pulse. The strength of this shock wave is a function of the closure configuration. The following paragraphs describe the design of the noise suppressing closures with various aerodynamic shapes, the tests conducted to determine the peak noise generated by each configuration and the test data analyses.

2.1 NOISE SUPPRESSING NOZZLE CLOSURE DESIGN

The noise produced by the nozzle closure being expelled from the throat of a nozzle is dependent on the velocity of the closure, the shape of the closure, the motor chamber pressure when the plug is released, and the cross section area of the closure that displaces the gas that it is passing through. If we make the assumption that the closures are stable for a short distance from the nozzle, the cross sectional area for each closure is the same and will not need to be considered as a variable. Since the velocity of the plugs was unknown, both subsonic and supersonic shapes were designed to weaken the shockwave produced. This was accomplished by using blunt, ogive and cone aerodynamic shapes. The closures with the blunt nose and aerodynamic base are designed for a subsonic closure velocity with a supersonic exhaust gas overtaking from the rear. The closures with the aerodynamic shapes on the nose are designed for the case where the closure velocity is just supersonic but slightly higher velocity than the exhaust gas. The closures with the aerodynamic shapes

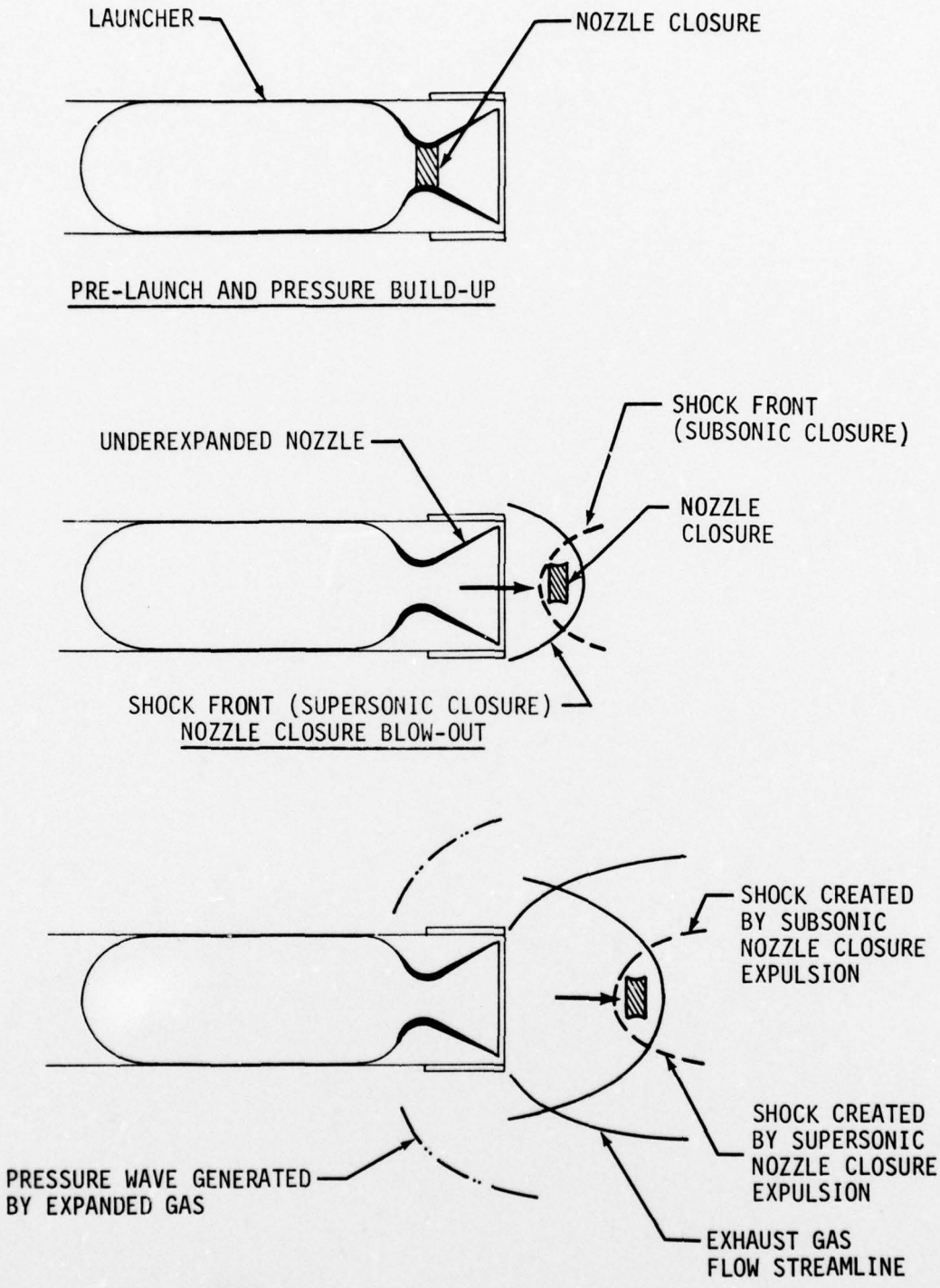

FIGURE 2-1. PRINCIPAL PEAK NOISE CONTRIBUTORS DURING FIRING OF A SMALL ROCKET MOTOR

2.1 (Continued)

on both the nose and base are designed for a supersonic closure velocity being overtaken by a supersonic exhaust gas velocity. Each aerodynamic configuration is shown in Figure 2-2. The pressure sealing flange used on these noise suppressing closures was designed to shear at the desired motor chamber pressure leaving a "clean" aerodynamic closure shape that is expelled from the nozzle. Detail drawings of the closures are given in Appendix A.

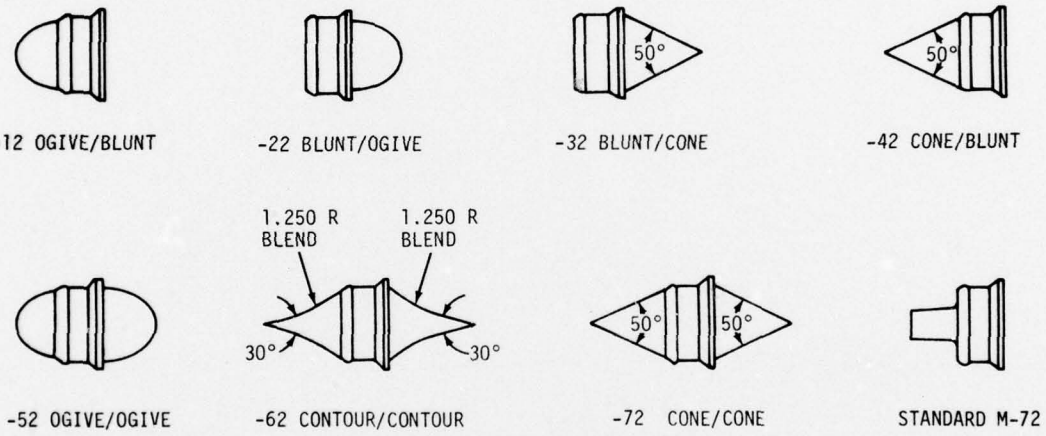

FIGURE 2-2. NOISE SUPPRESSING CLOSURES

2.2 NOISE SUPPRESSING NOZZLE CLOSURE RELEASE PRESSURE TEST

The noise suppressing closures do not have the ignitor cavity in the base as the standard M-72 closure. This design difference was expected to cause the noise suppressing closures to release at higher motor chamber pressure than the standard M-72 closure. A special test was planned and executed that would determine the release pressure of all the closure designs. In order to test for release pressure, the special test fixture shown in Figure 2-3 was designed and fabricated by MIRADCOM. The test

2.2 (Continued)

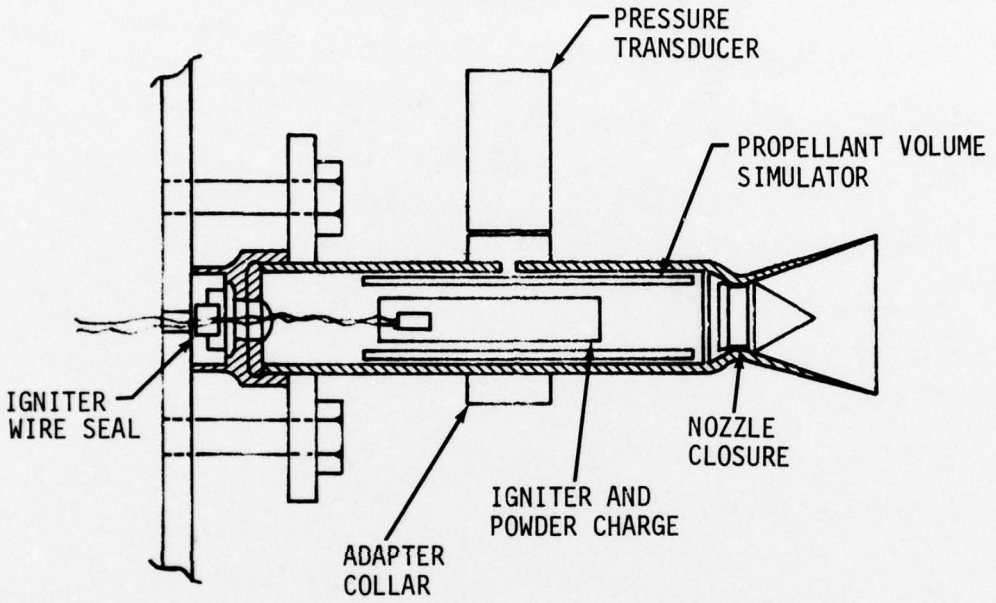

FIGURE 2-3. NOZZLE CLOSURE RELEASE PRESSURE TEST FIXTURE

fixture is made up of a modified M-72 motor that can be attached to the wall of the test cell. MIRADCOM also designed and fabricated special ignitors capable of raising the motor chamber pressure to 6000 psia. This ignitor was used to generate gasses that would simulate the actual M-72 rocket motor chamber pressure buildup rate prior to closure expulsion. No propellant, other than the ignitor, was used in the release pressure tests. An inert cylinder was installed in the motor chamber to simulate the initial propellant volume prior to ignition so that chamber pressure buildup rates would be more realistic. Chamber pressure was measured with a pressure transducer attached to the collar clamped to the motor case. A hole was drilled through the motor case under the pressure transducer. The ignitor wires were routed out through a head end seal so that they would not have to be routed through the nozzle closures.

2.2 (Continued)

Using the test fixture described above, the initial nozzle closure release pressure tests were conducted with the standard M-72 nozzle closure. Data for chamber pressure as a function of time was recorded on magnetic tape and on an oscillograph. The peak pressure from these data are recorded for each test in Table 2-I.

TABLE 2-I - STANDARD M-72 NOZZLE CLOSURE RELEASE PRESSURE

Test No.	Release Pressure PSIA
3	1215
4	1125
5	1237
6	997.5
7	1020
8	1162
9	1087.5
10	1050
11	1207.5
12	1057.5
13	1300
14	1050
15	1040

The average release pressure for the standard M-72 nozzle closure from the data in Table 2-I is 1119.2 psia. This average release pressure was used as the baseline release pressure for designing the flange on the noise suppressing closures. The standard M-72 closure flange was duplicated on each of the noise suppressing closure configurations. Initial tests of the noise suppressing closures revealed that they would not release at

2.2 (Continued)

pressures above 2500 psia. The flange configuration was modified as shown in Figure 2-4(a) by removing .032 inches of the aft portion of the flange. This modified flange configuration would not allow the closure to release at pressures up to 2500 psia. The flange configuration was further modified as shown in Figure 2-4(b) by undercutting the flange to a depth of .11 inches. This flange configuration had a root thickness of .065 inches and expelled at a peak motor chamber pressure of 1850 psia. The flange configuration was modified again with more undercutting of the flange to a depth of .135 inches as shown in Figure 2-4(c). The flange root thickness of the

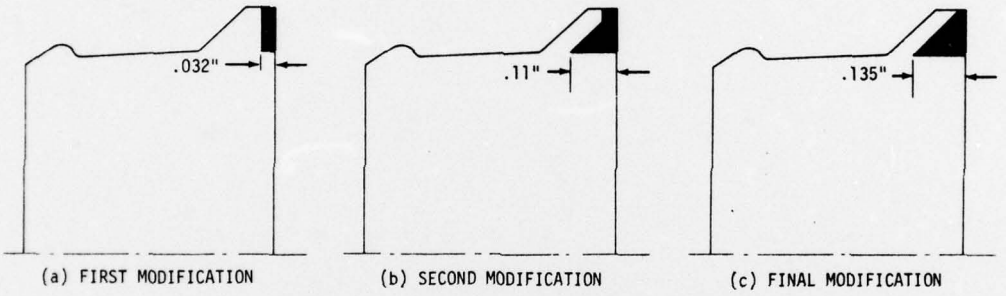

FIGURE 2-4. FLANGE MODIFICATION

final modification was .040 inches. Five noise suppression closure configurations were modified to the .040 flange root thickness. The peak release pressure of each of these closures was determined and the results are given in Table 2-II.

TABLE 2-II - NOISE SUPPRESSING CLOSURE RELEASE PRESSURE

Configuration .040 Flange Root	Release Pressure PSIA
-12 ogive/blunt	840
-42 cone/blunt	920
-52 ogive/ogive	1030
-62 contour/contour	970
-72 cone/cone	960

2.2 (Continued)

The trend data for plug release pressure for the flange root thickness tested is shown in Figure 2-5. Using these data it was determined that a noise suppressing closure flange root thickness of .047 inches would produce a mean release pressure of 1200 psia. Each of the noise suppressing closure configurations was fabricated with a flange root thickness of .047 inches for the nozzle closure tests.

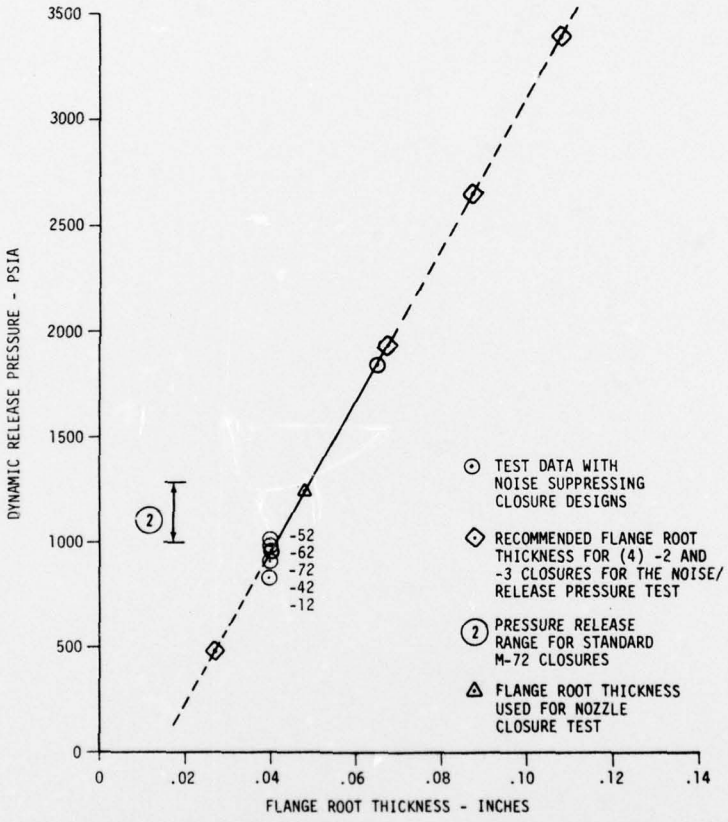

FIGURE 2-5. NOISE SUPPRESSING CLOSURE RELEASE PRESSURE

By extrapolating the data for release pressure versus flange root thickness given in Figure 2-5, it can be determined that the noise suppressing closure can be modified to allow testing over a wide range of release pressures. Since the flange shears free leaving a "clean" aerodynamic shape that is expelled, it was determined that release pressure would be the only variable in such a test. Four release pressure levels were selected, three

2.2 (Continued)

above and one below the standard 1200 psia as shown on Figure 2-5. The noise suppressing closure configurations selected for the release pressure test were the -22 (blunt/ogive) and the -32 (blunt/cone). These are shown in Figure 2-6.

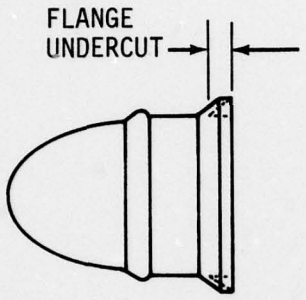

CONFIGURATION	FLANGE UNDERCUT (INCHES)
-23 OGIVE/BLUNT	.148
-24 OGIVE/BLUNT	.108
-25 OGIVE/BLUNT	.088
-26 OGIVE/BLUNT	.068

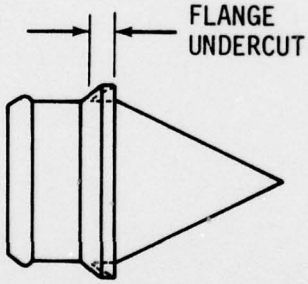

CONFIGURATION	FLANGE UNDERCUT (INCHES)
-33 BLUNT/CONE	.148
-34 BLUNT/CONE	.108
-35 BLUNT/CONE	.088
-36 BLUNT/CONE	.068

FIGURE 2-6. NOISE SUPPRESSING CLOSURES FOR THE RELEASE PRESSURE TEST

2.3 NOISE SUPPRESSING NOZZLE CLOSURE TEST

Each of the noise suppressing closure configurations developed through the design and test described in paragraphs 2.1 and 2.2 were fired in a simulated launch situation to determine their noise suppressing capability. The test fixture used for this test is shown in Figure 2-7. Special design

2.3 (Continued)

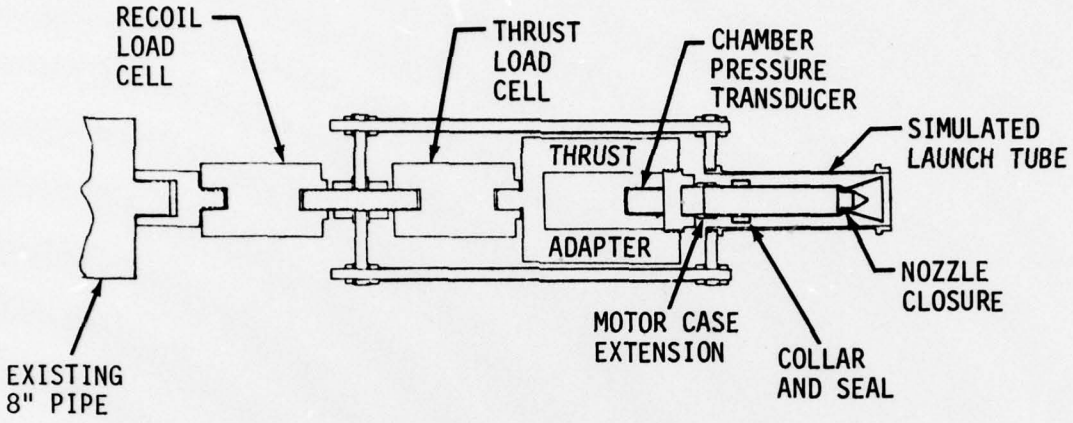

FIGURE 2-7. NOZZLE CLOSURE TEST FIXTURE

features of this fixture include a dual load cell arrangement for measuring both recoil and thrust. The motor case is modified with a collar and seal that allows the ignitor wires to exit through the case rather than the closure. The forward end of the motor case is extended so that the various closure designs will not interfere with the propellant and special bag ignitor. Detail drawings of this test fixture are given in Appendix A. This test fixture was installed in the Propulsion Directorate Small Rocket Test Facility as shown in Figure 2-8. The instrumentation for this test included measurements for thrust, recoil, motor chamber pressure and sound pressure level. Instrumentation locations are shown in Figure 2-7 for all variables except sound pressure level gages which are located as shown in Figure 2-9.

A typical motor buildup, installation and test sequence included the following items.

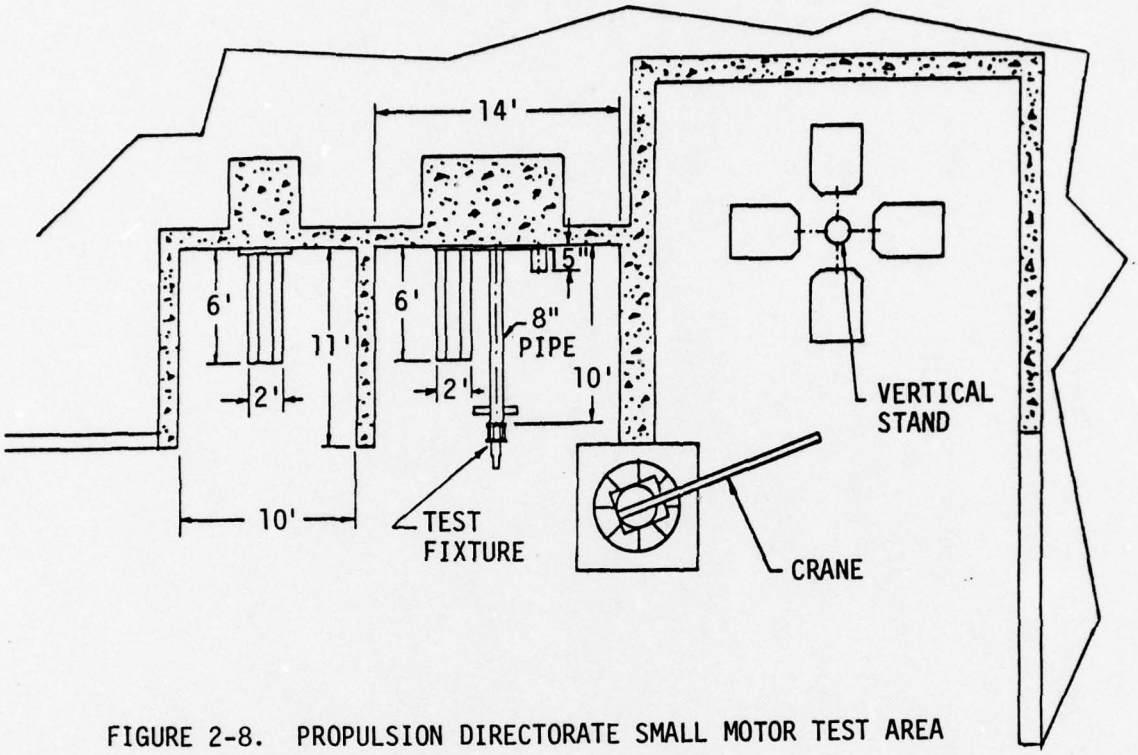

FIGURE 2-8. PROPULSION DIRECTORATE SMALL MOTOR TEST AREA

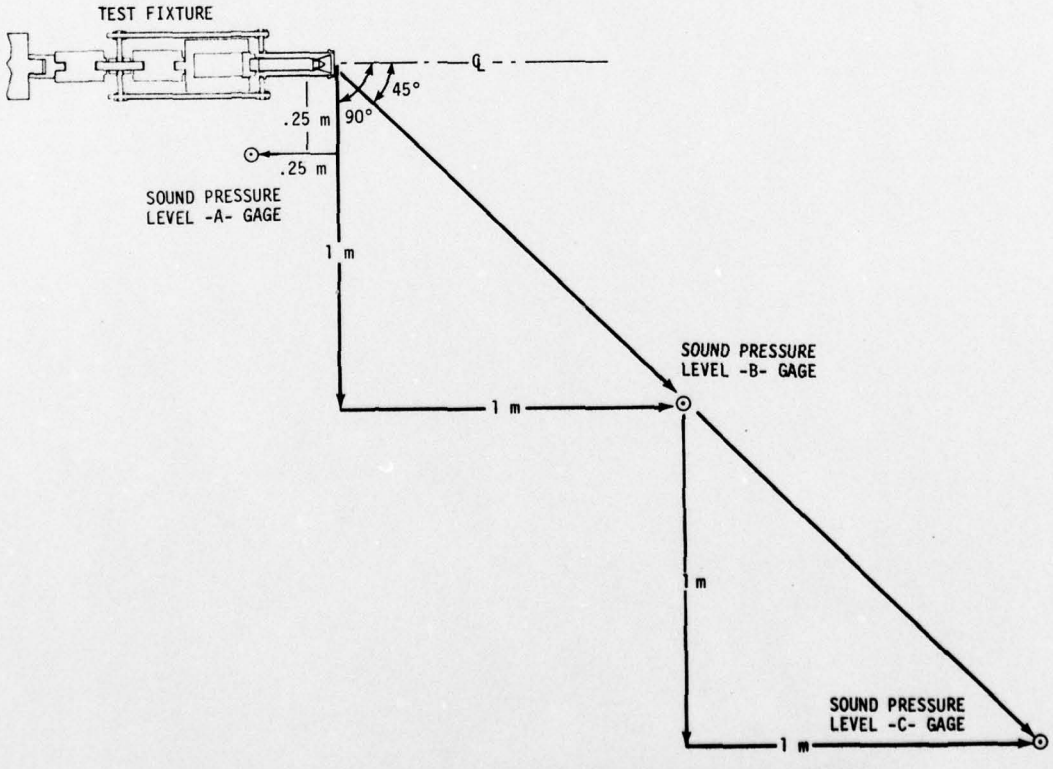

FIGURE 2-9. SOUND PRESSURE LEVEL GAGE LOCATIONS

2.3 (Continued)

1. Install the nozzle closure in the throat of the nozzle.
2. Install the bag ignitor.
3. Route the ignitor wires through the case and collar seal.
4. Load the motor with standard M-72 propellant.
5. Check instrumentation for operation.
6. Install the motor in the test fixture.
7. Fire Motor and Record data

The data measured by the instrumentation was recorded on both magnetic tape and on an oscillograph recorder for the duration of the motor firing. A typical oscillograph recording of the data is shown in Figure 2-10.

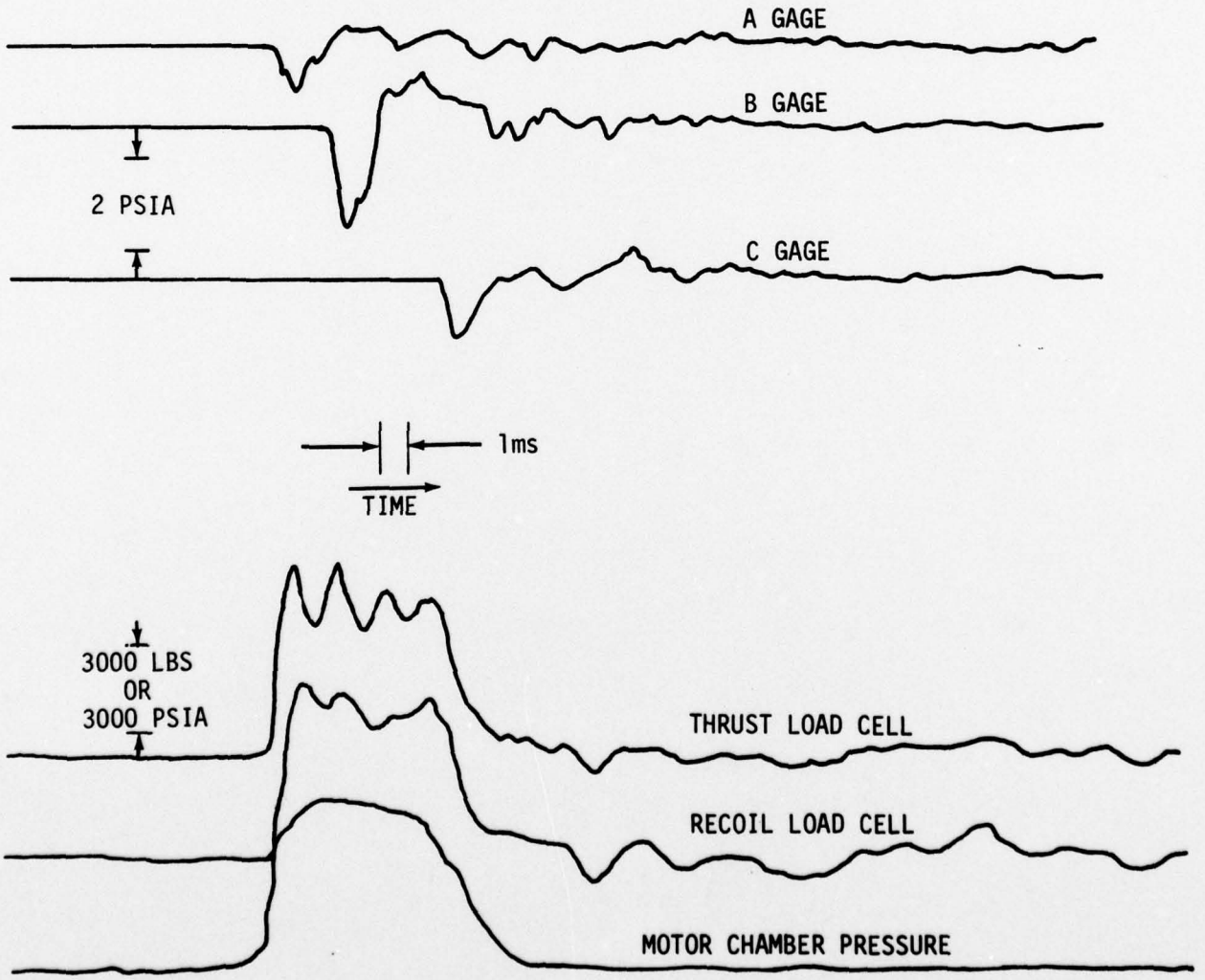

FIGURE 2-10. OSCILLOGRAPH DATA RECORDED DURING THE NOZZLE CLOSURE TESTS

2.4 NOISE SUPPRESSING NOZZLE CLOSURE TEST DATA ANALYSIS

The peak sound pressure level data recorded for each of the noise suppressing closure configurations tested are presented in Table 2-III. These data were developed from the oscillograph data as follows. Using the oscillograph trace for the A gage in Figure 2-10 as example, the recorded data for A gage reads zero until the pressure wave passes. The initial peak pressure level recorded as the pressure passed the gage has been interpreted as the peak sound pressure level.

The data for a series of five standard M-72 closures that are presented in Table 2-III were used to determine the baseline levels for the sound pressure gages at positions A, B, and C shown in Figure 2-9. These data indicate that the sound pressure level at each position is unaffected by motor-to-motor variations. This hypothesis is further supported by the data shown in Figure 2-11 that shows that peak noise produced at each position is virtually unaffected by peak thrust.

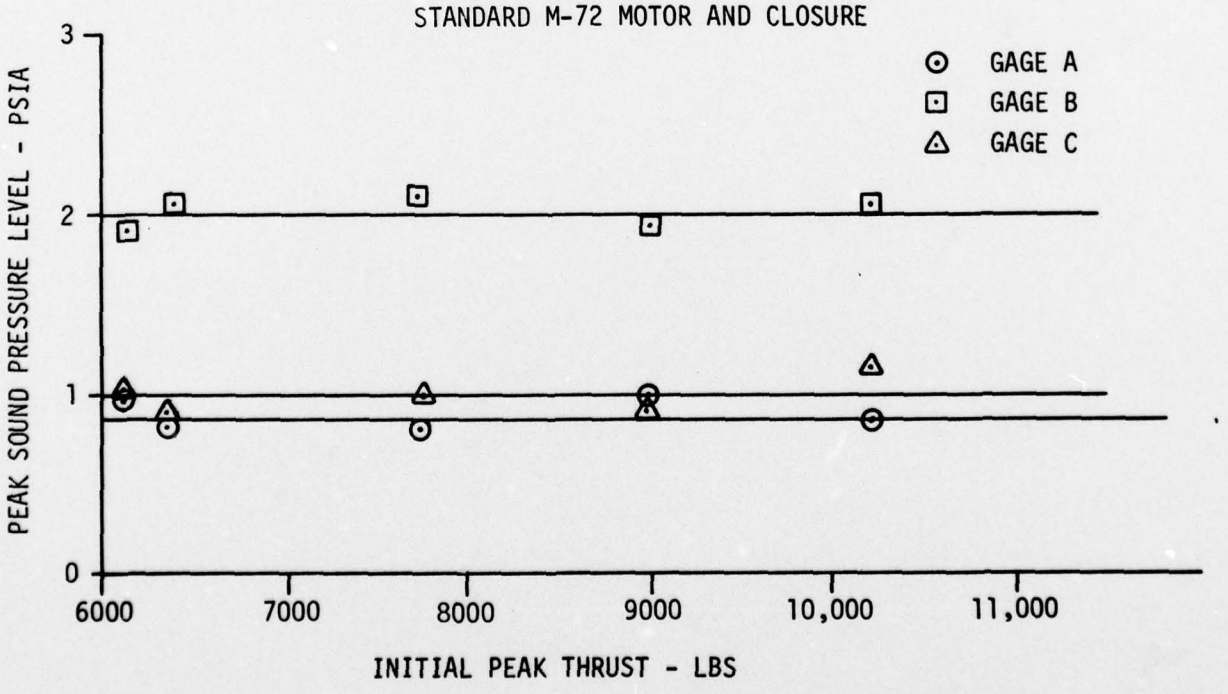

FIGURE 2-11. MOTOR-TO-MOTOR VARIATION OF PEAK SOUND PRESSURE LEVELS

TABLE 2-III - NOZZLE CLOSURE PEAK SOUND PRESSURE LEVEL DATA

CLOSURE CONFIGURATION	A GAGE		B GAGE		C GAGE	
	P - PSIA	db*	P - PSIA	db*	P - PSIA	db*
-12 Ogive/Blunt	.92	170.05	1.98	176.75	1.16	172.05
-22 Blunt/Ogive	1.0	170.75	2.68	179.25	.98	170.6
-32 Blunt/Cone	1.28	173	2.32	178.05	1.36	173.4
-33 Blunt/Cone	1.14	171.95	2.06	177.05	.98	170.6
-34 Blunt/Cone	1.68	175.35	2.2	177.6	1.08	171.5
-35 Blunt/Cone	1.22	172.5	1.96	176.6	1.1	171.6
-36 Blunt/Cone	1.14	171.8	1.92	176.45	1.08	171.5
-42 Cone/Blunt	1.36	173.45	1.68	175.35	1.38	173.6
-52 Ogive/Ogive	1.24	172.65	1.90	176.35	1.10	171.6
-62 Contour/Contour	1.04	171.1	1.86	176.15	1.24	172.65
-72 Cone/Cone	1.16	172.0	1.70	175.4	1.24	172.65
-12 Ogive/Blunt	.74	168.1	2.1	177.2	.88	169.7
-12 Ogive/Blunt	.66	167.1	2.02	176.9	.88	169.7
-12 Ogive/Blunt	.86	169.5	1.84	176.1	.86	169.5
-12 Ogive/Blunt	.74	168.1	2.06	177.0	.88	169.7
-12 Ogive/Blunt	.8	168.9	1.92	176.4	.94	170.25
-22 Blunt/Ogive	.86	169.5	2.12	177.3	.82	169.1
-22 Blunt/Ogive	.72	167.9	2.08	177.1	.9	169.9
-22 Blunt/Ogive	.8	168.9	2.32	178.1	.94	170.25
-22 Blunt/Ogive	.78	168.6	2.42	178.4	.92	170.1
-22 Blunt/Ogive	1.08	171.5	2.3	178	.86	169.5
-23 Blunt/Ogive	.68	167.5	1.92	176.4	.76	168.4
-24 Blunt/Ogive	.9	169.9	1.8	175.9	1.0	170.8
-25 Blunt/Ogive	.82	169.1	2.24	178.3	.9	169.9
-26 Blunt/Ogive	.76	184.4	2.06	177	.94	170.3
Standard M72	.8	168.85	2.1	177.2	1.0	170.75
Standard M72	1.0	170.75	1.94	176.5	.92	170.05
Standard M72	.84	169.3	2.02	176.9	1.14	171.9
Standard M72	.96	170.4	1.92	176.4	1.02	170.9
Standard M72	.8	168.85	2.06	177.1	.9	169.9

*$db = 20 \text{ LOG}_{10} \frac{P}{2 .9008 \times 10^{-9}}$

2.4 (Continued)

Since the peak sound pressure levels measured at position A, B, and C had small motor-to-motor variations for the five standard M-72 closures tested, the baseline sound levels were developed by averaging the data for these positions. The average sound pressure level and standard deviation data for the standard M-72 that will be used throughout this report as a baseline are given in Table 2-IV.

TABLE 2-IV. STANDARD M-72 PEAK SOUND PRESSURE LEVEL DATA

GAGE POSITION	AVERAGE SOUND PRESSURE DATA		STANDARD DEVIATION
	P - PSIA	DB*	σ
A	0.88	169.7	±.0938
B	2.0	176.8	±.0769
C	0.996	170.8	±.0953

$$*DB = 20 \text{ LOG}_{10} \frac{P}{2.9008 \times 10^{-9}}$$

With the baseline sound pressure levels established above as a reference, the data for the noise suppressing closure configurations were evaluated for peak noise reduction capability. The data presented in Table 2-III revealed that none of the noise suppressing closure configurations designed for 1200 psia release pressure are quieter than the standard M-72 closure at the gunners position (A gage). Configurations -12 (ogive/blunt) and -22 (blunt/cone) are the quieter of the six designs. In order to reduce the motor-to-motor effects on peak noise, five each of the two quieter closure designs were fired in a repeat test. The results of this test shows that the -12 configuration on the average was 1.3 db quieter than the standard plug at the gunners position (A gage). The -22 configuration was only 0.4 db quieter.

2.4 (Continued)

A separate analysis of the data generated for the noise suppressing closures designed for different release pressure was made. This analysis revealed that medium release pressure levels produced the highest peak noise levels as shown in Figure 2-12. The spread in the data for the two configurations at the A gage position is too large for a motor-to-motor variation. These differences have been attributed to instrumentation accuracy or calibration. The trends in the data show that the lower release pressures tend to produce lower peak noise at all three sound pressure level gage positions.

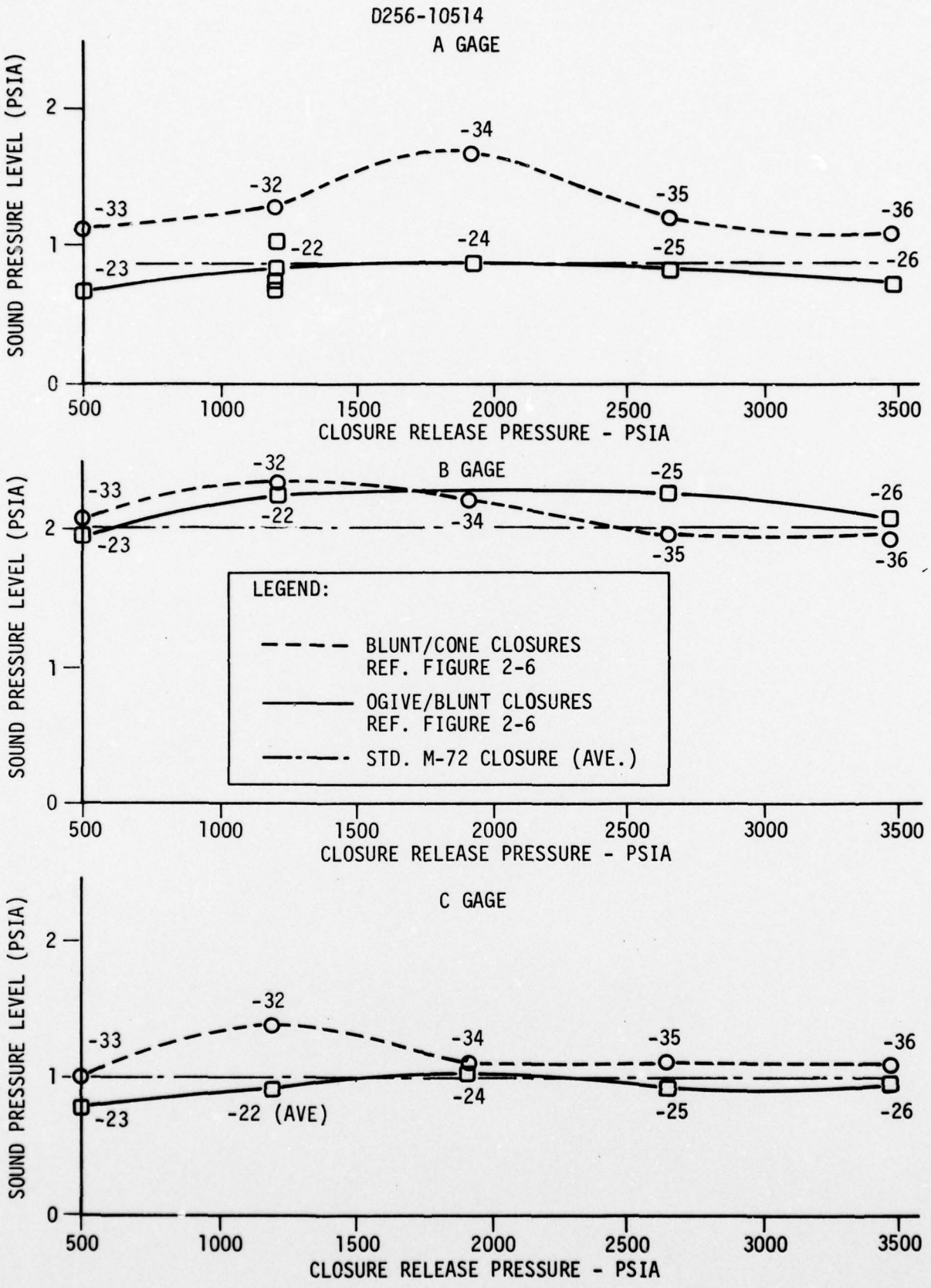

FIGURE 2-12. PEAK NOISE FOR SEVERAL RELEASE PRESSURES

3.0 NOISE SUPPRESSOR DESIGN AND EVALUATION

Following the noise suppressing closure tests the Peak Noise Reduction Program was continued by developing a technique that would weaken peak noise associated with the nozzle closure motion and the pressure wave created by the exhaust gasses leaving the nozzle. The gas flow model was assumed to be similar to the gas flow/projectile relationship shown in Figure 3-1. An effective suppressor must weaken the pressure and shock waves of the type shown in Figure 3-1 as early in their formation as possible with minimum effect on rocket performance and launcher recoil. The following paragraphs will discuss the design and test of peak noise suppressors that intercept and weaken the pressure and shock waves by use of controlled gas expansion, shock baffling, energy diffusion and noise focusing.

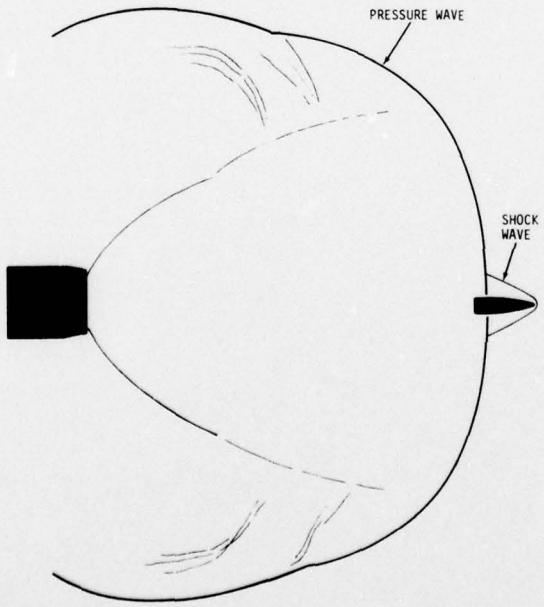

FIGURE 3-1. SHOCK WAVES PRODUCED 400 μSEC AFTER FIRING A .30 CALIBER BULLET (FROM REFERENCE 2)

3.1 NOISE SUPPRESSOR DESIGN

The peak noise produced by a rocket motor firing is associated with the pressure and shock waves illustrated in Figure 3-1. When these waves pass the gunners position they have attenuated some due distance traveled from the apparent emitter but are still strong enough to create a .88 psia overpressure at the gunners position as shown in Table 2-IV for the standard M-72 motor.

Several suppressor concepts for weakening these pressure waves before they reach the gunners position were tested and the results reported in Reference 1. Of the configurations tested, the baffled cylinder design was the most effective noise reducer. This concept is shown in simplified form in Figure 3-2. The concept allows the strong pressure wave that occurs as the nozzle closure is expelled from the nozzle to expand up to the baffle. When the pressure wave reaches the baffle, part of the wave is reflected and part is allowed to pass through the orifice. The expansion-reflection process weakens the pressure wave and must be repeated in three chambers to maximize the effectivity of the baffled cylinder suppressor.

The two suppressors shown in Figure 3-3 were designed to evaluate the capability of the baffled cyclinder concept to reduce the noise produced by the M-72 weapon system. These suppressors were designed to evaluate the concept and were not intended to approach a field weight system. The inside diameters of the two suppressors were set at eight (8) inches and ten (10) inches. Each suppressor was designed so that, by selecting a combination of the cylinder sections shown in Figure 3-4, the chamber length between the baffles could be varied from one inch to six inches in one inch intervals. Bosses were installed in each two and three inch cylinder sections for installation of pressure transducers. The orifice size of the baffles could be varied from 2.55 inches to 4 inches and in addition both rigid and yielding baffles shown in Figure 3-5 were fabricated. The cylinder sections and baffle conbinations were held together with a four piece band clamp shown in Figure 3-6. To determine the effects of perforations in the cylinder between the baffles, a perforated cylinder segment is shown separated and installed in a suppressor in Figure 3-7. Detailed design drawings of the suppressors are included in Appendix A.

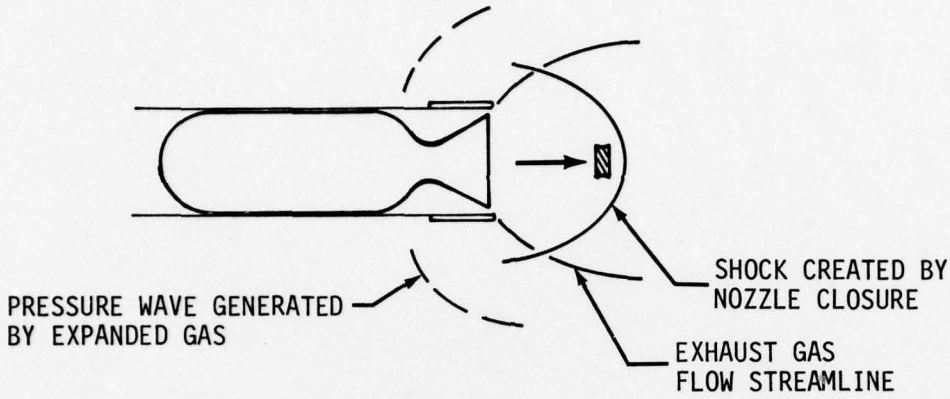

NORMAL NON-IMPEDED GAS FLOW CHARACTERISTICS

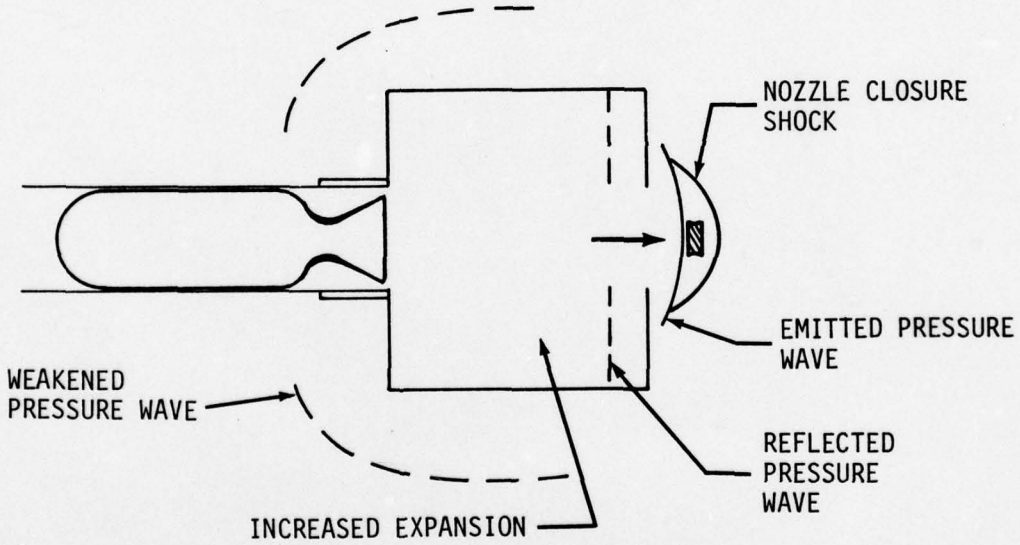

BAFFLED GAS FLOW CHARACTERISTICS

FIGURE 3-2. BAFFLED CYLINDER SUPPRESSOR CONCEPT

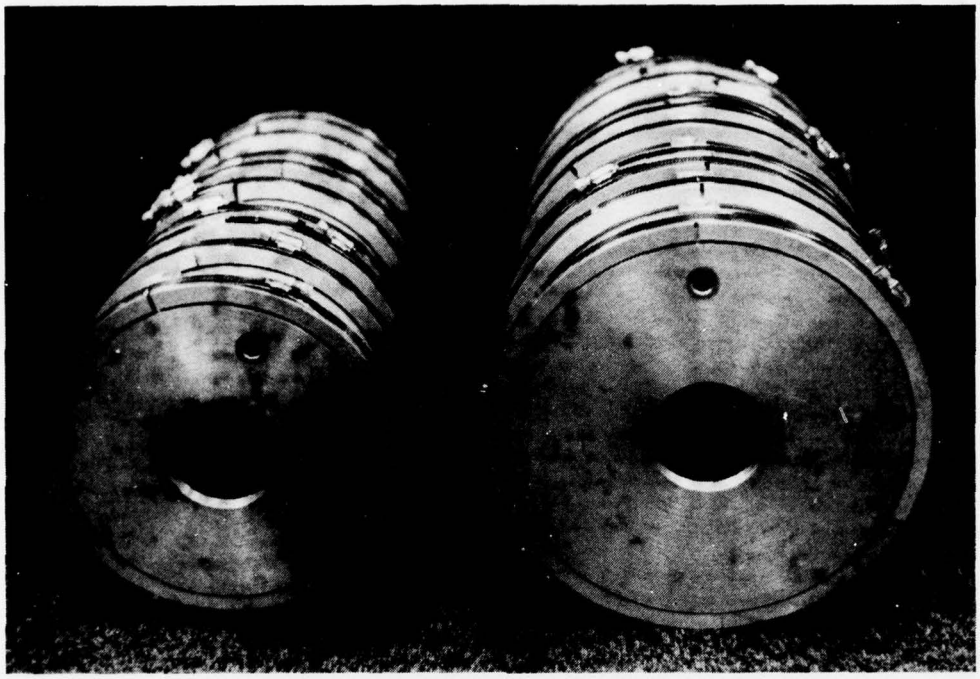

8" ID SUPPRESSOR 10" ID SUPPRESSOR

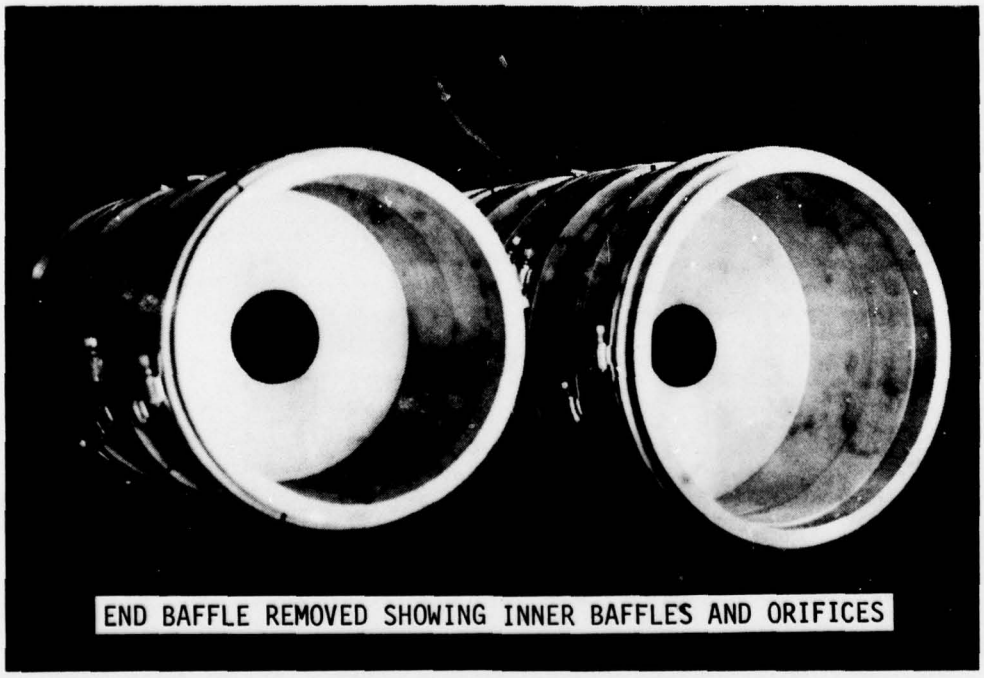

FIGURE 3-3. BAFFLED CYLINDER SUPPRESSOR

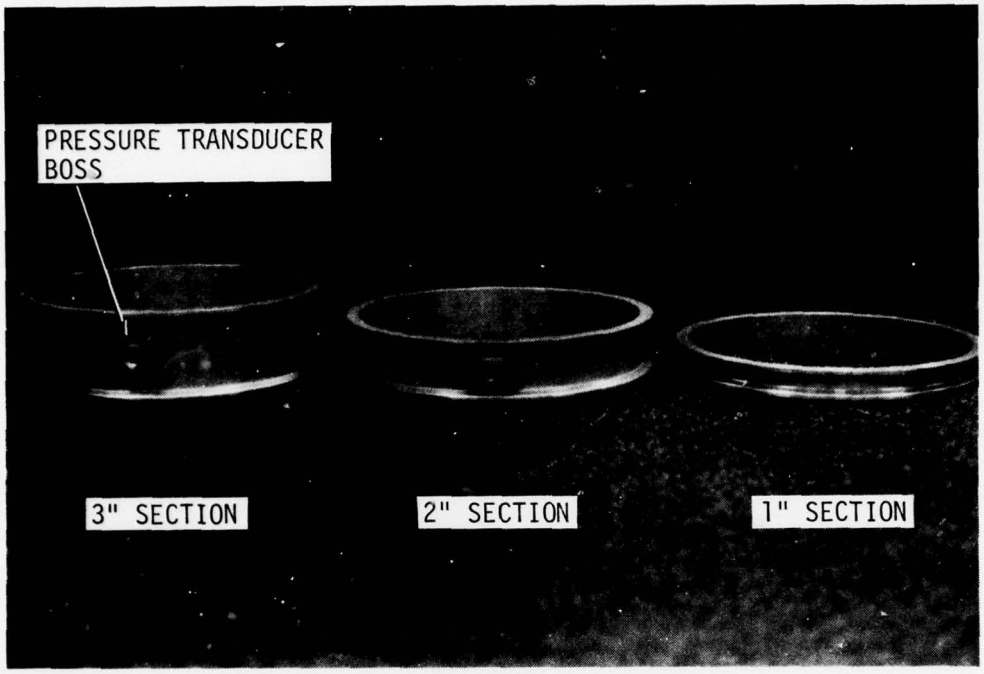

FIGURE 3-4. SUPPRESSOR CYLINDER SECTIONS

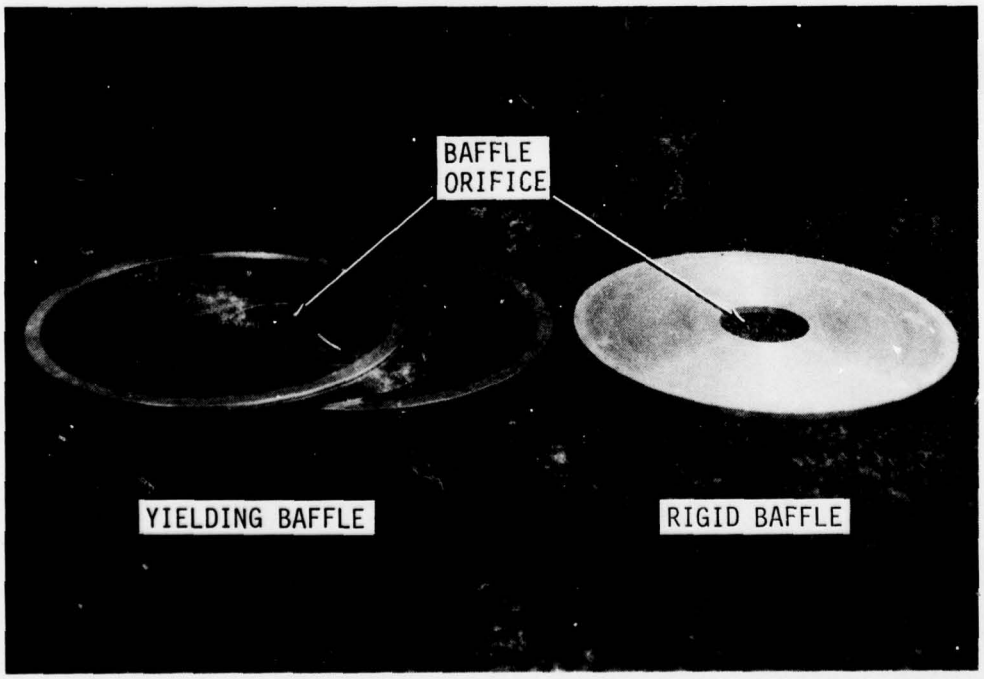

FIGURE 3-5. NOISE SUPPRESSOR BAFFLES

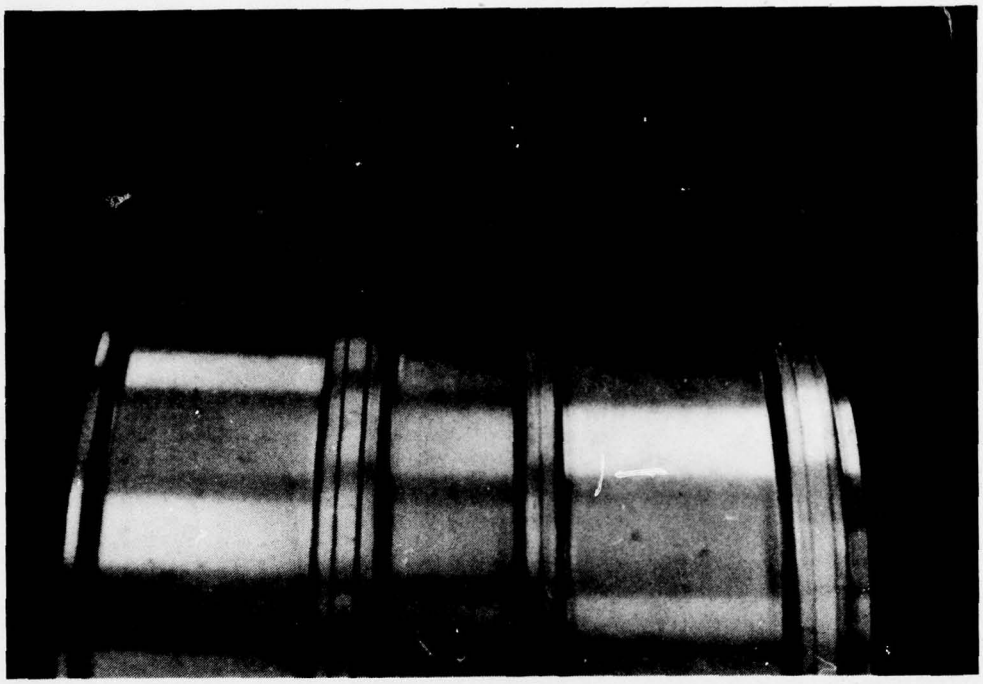

BAND CLAMP INSTALLATION

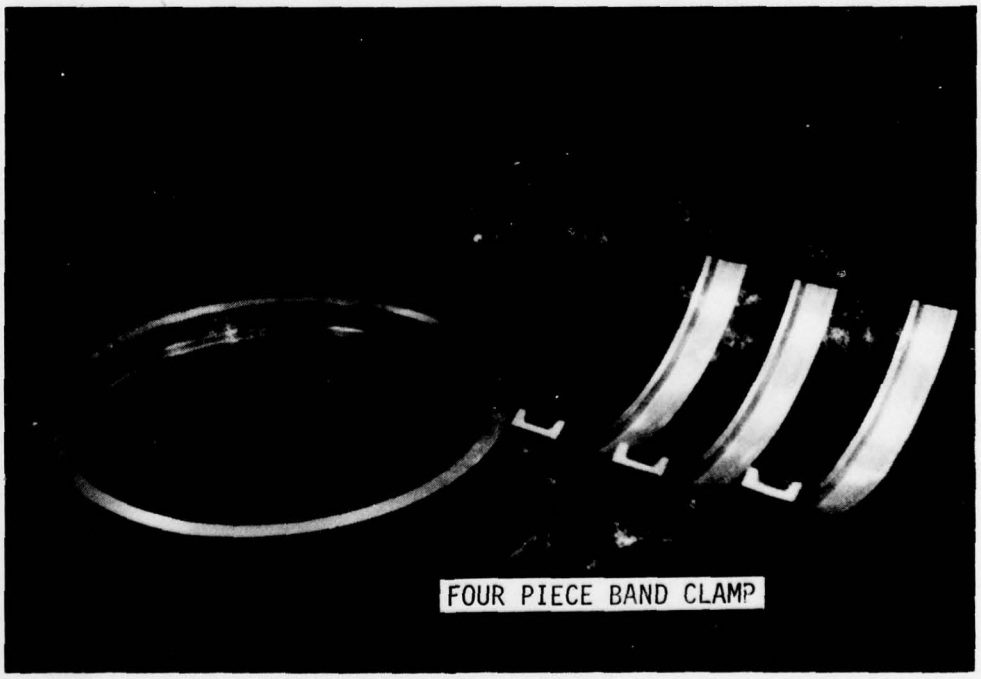

FIGURE 3-6. SUPPRESSOR BAND CLAMP

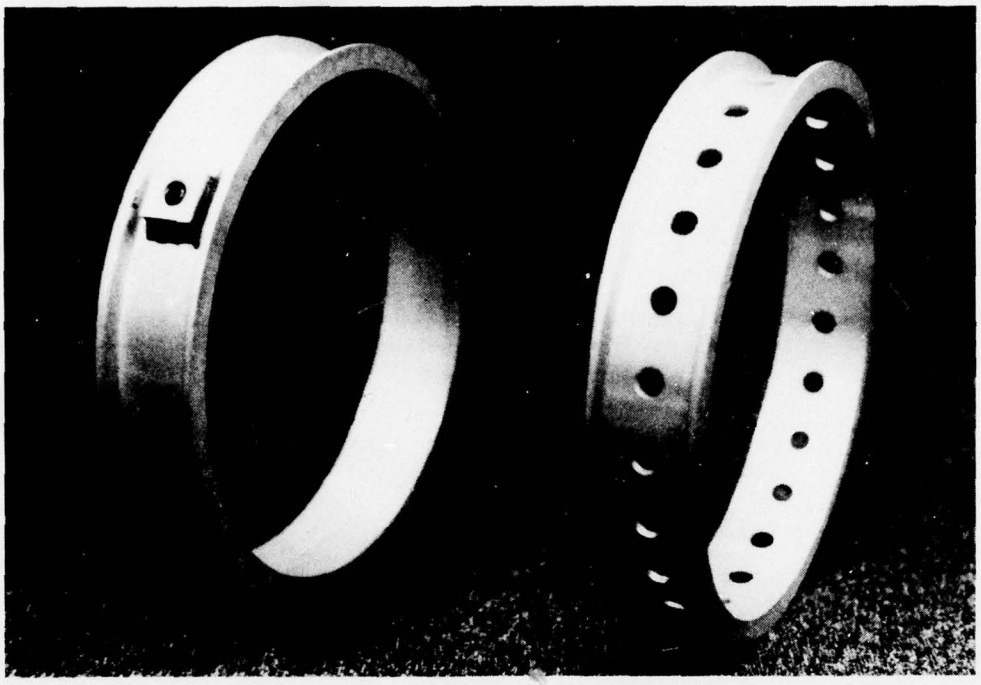

STANDARD SEGMENT PERFORATED SEGMENT

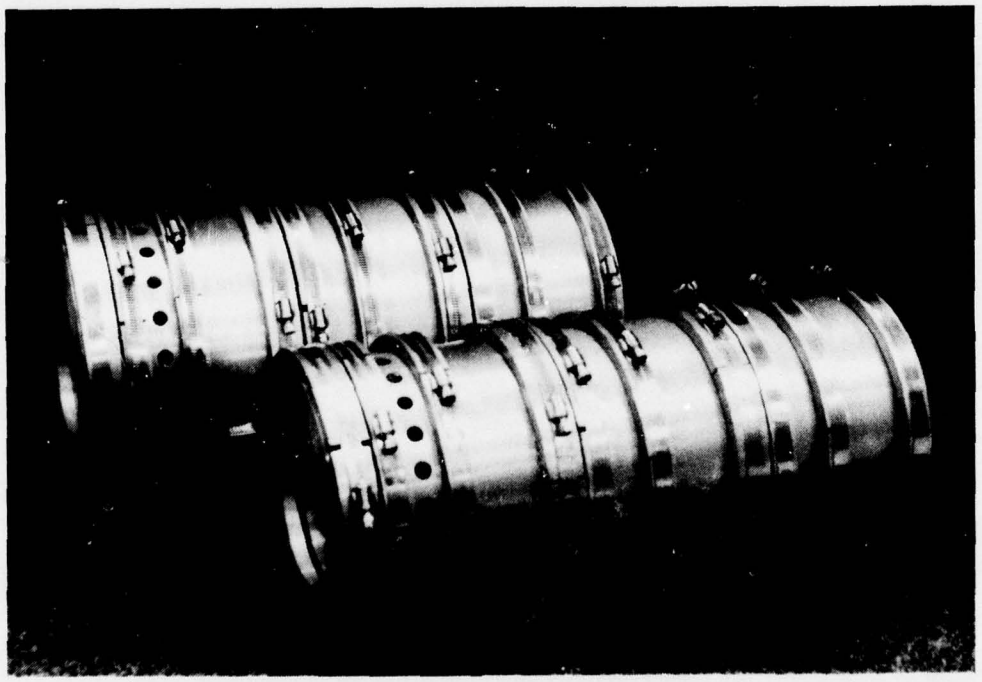

FIGURE 3-7. PERFORATED CYLINDER SUPPRESSORS

3.2 SUPPRESSOR TEST

The forward end plates of the suppressors were designed to attach to the aft end of the test fixture described in paragraph 2.3. Figure 3-8 shows a suppressor attached to the test fixture. This installation utilized all the existing features of the test fixture including the instrumentation. When the suppressor is attached, three suppressor chamber pressure transducers are added to the instrumentation used for the Noise Suppressing Closure Test shown in Figures 2-7 and 2-9. The M-72 rocket motor used for this test was identical to that used for the noise suppressing closure test and included the special collar seal and the motor case extension.

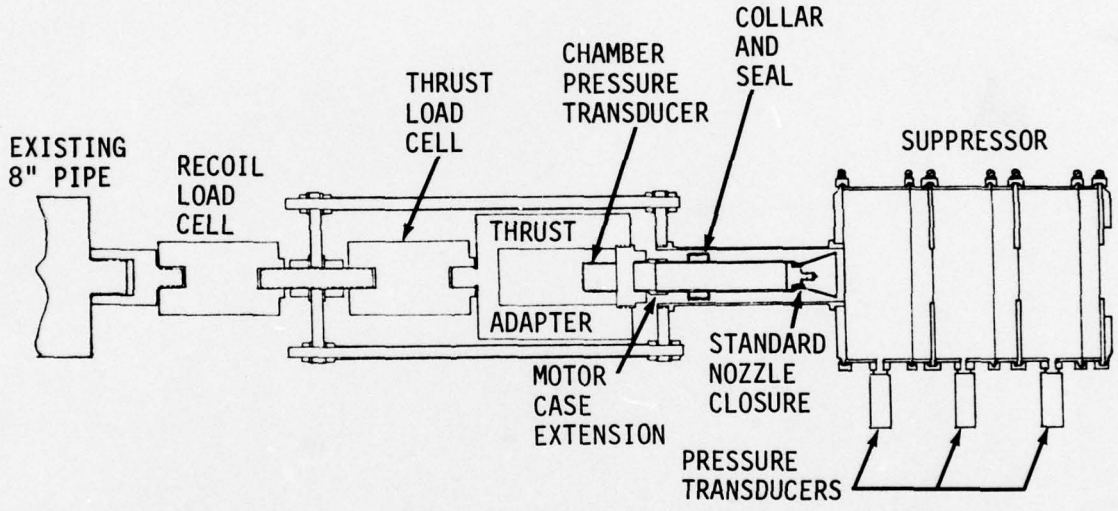

FIGURE 3-8. NOISE SUPPRESSOR TEST FIXTURE

A typical test sequence was identical to that described in paragraph 2.3 for the nozzle closure test up to motor installation. While the motor was being assembled and installed, the suppressor configuration was assembled from cylinder sections, baffles and end plates and secured with the band clamps. The suppressor was installed on the aft end of the simulated launch tube after the rocket motor was in place. The instrumentation was checked and the motor was fired. Data for each instrumented variable was recorded on magnetic tape and on a recording oscillograph for the duration of each

3.2 (Continued)

firing. Typical oscillograph recordings of this data are shown in Figures 3-9 and 3-10. The sound pressure level, thrust, recoil and motor chamber pressure data are shown in Figure 3-9. A separate recording of the suppressor chamber pressure was necessary and is shown in Figure 3-10.

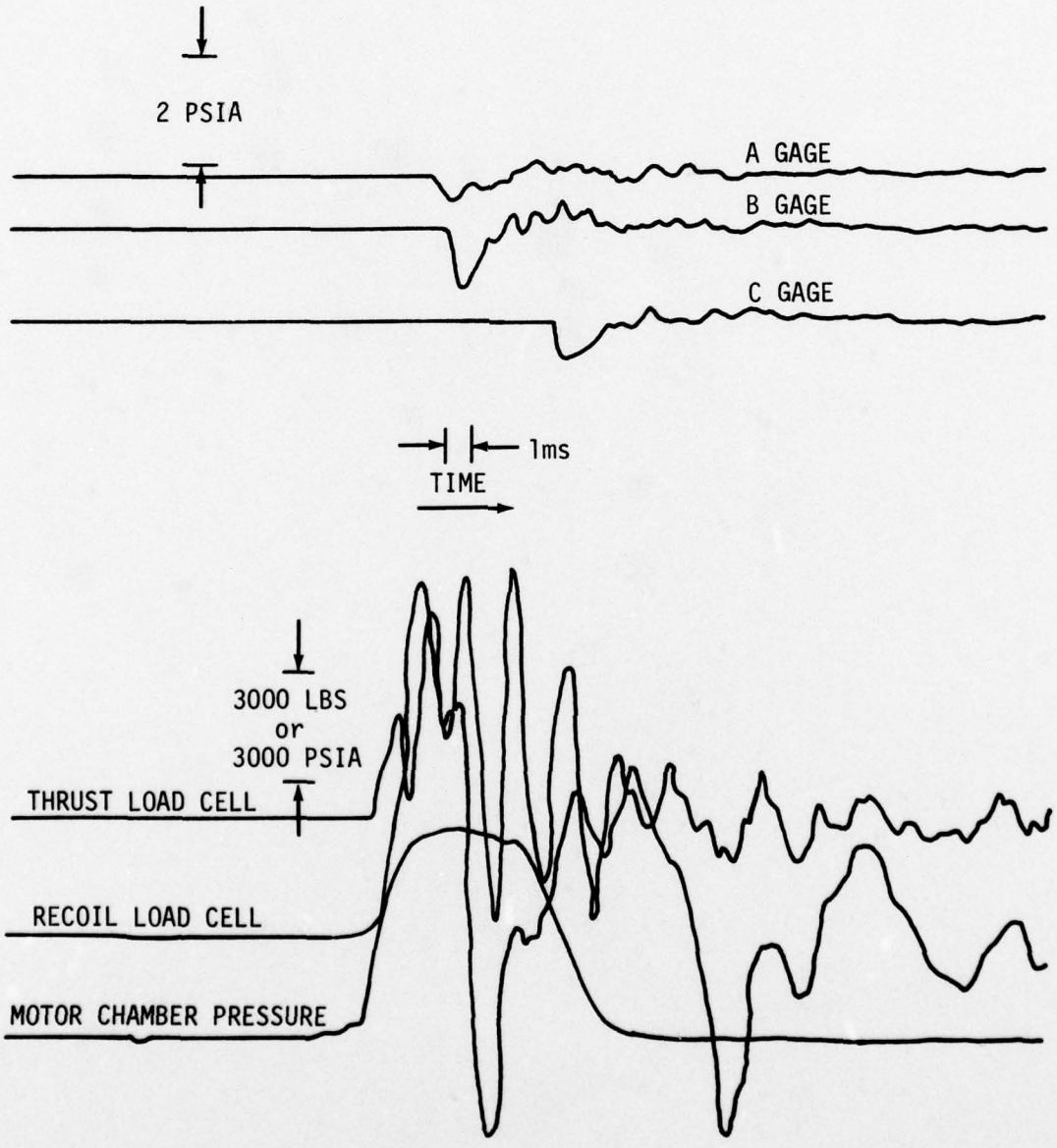

FIGURE 3-9. OSCILLOGRAPH DATA RECORDED DURING THE NOISE SUPPRESSOR TESTS (PART 1)

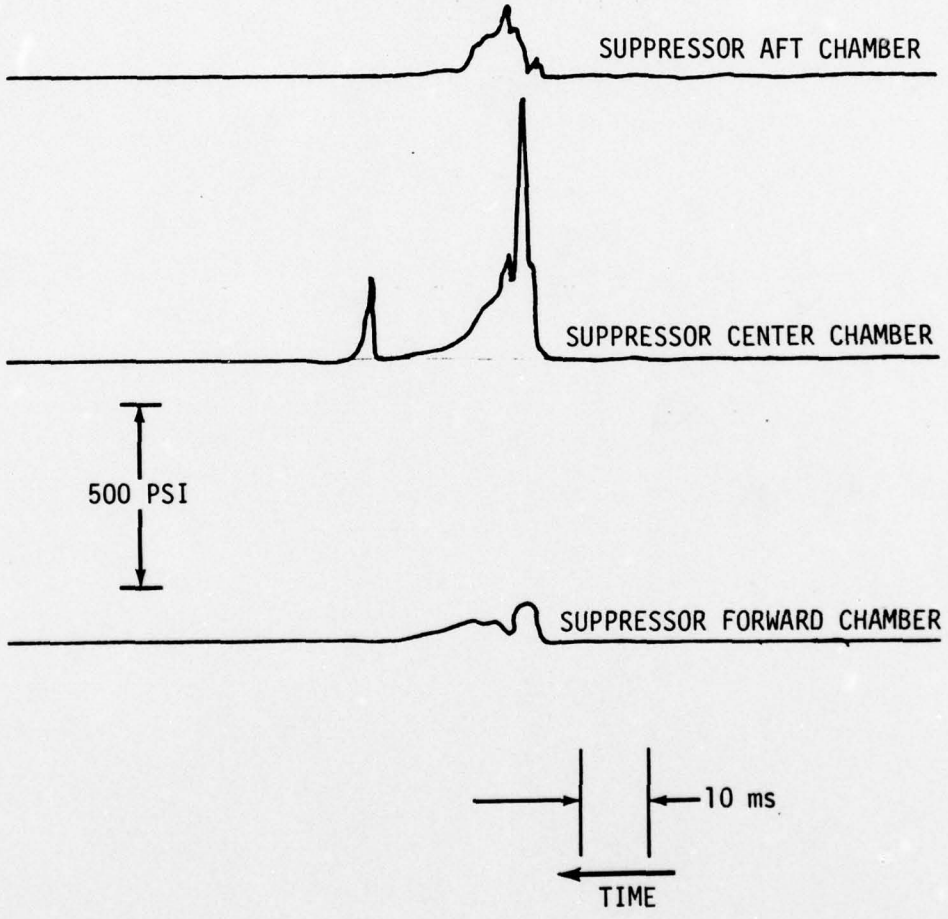

FIGURE 3-10. OSCILLOGRAPH DATA RECORDED DURING THE NOISE SUPPRESSOR TESTS (PART 2)

3.3 SUPPRESSOR TEST DATA ANALYSIS

The suppressor test data analysis has been approached from several aspects. The data has been analyzed to determine the capabilities of the suppressor to reduce the peak noise produced by a small rocket motor and to determine the effects of the suppressor on rocket motor performance and launcher recoil. An indepth data analysis, which is presented in paragraph 4.0, was performed to understand the character of the sound field produced by a rocket motor firing and the mechanism of energy absorbed by the suppressor.

3.3.1 Noise Suppressor Capabilities

The typical sound pressure level data from gages A, B, and C given in Figure 3-9 show the characteristics of the measured data. The sound pressure levels remain at zero until the pressure wave passes the gage position. The initial peak associated with the pressure wave passing the gage has been interpreted as the peak sound pressure level. Each of these peak sound pressure levels are recorded in Table 3-I for all suppressor configurations tested. Using the data presented in Table 3-I suppressor capability data were developed in Figures 3-11, 3-12 and 3-13 for each of the three sound pressure level gage positions. By comparing the baseline sound pressure level established in paragraph 2.4 and the sound pressure levels measured with the suppressor installed, the overall capability of

TABLE 3-I. NOISE SUPPRESSOR PEAK SOUND PRESSURE LEVEL DATA

SUPPRESSOR CONFIGURATION (3 CHAMBERS)			GAGE POSITION						COMMENTS
INSIDE DIAMETER INCHES	CHAMBER LENGTH INCHES	ORIFICE SIZE INCHES	A		B		C		
			P ∿ PSIA	db*	P ∿ PSIA	db*	P ∿ PSIA	db*	
8	3	2.55	.4	162.8	1.56	174.6	--	--	Lost C gage data
8	4	2.55	.44	163.6	1.50	174.3	--	--	Lost C gage data
8	5	2.55	.32	160.9	1.56	174.6	--	--	Lost C gage data
8	6	2.55	.28	159.7	1.16	172.0	.62	166.5	
8	6	2.55Y	.26	159.1	1.14	171.9	.60	166.3	Yielding Baffles
8	6(1 Perf.)	2.55	.42	163.2	1.16	172.0	.68	167.4	Aft Chamber Perforated
8	6	3.0	.26	159.1	1.45	174.0	.62	166.5	
8	18	None	.68	167.4	1.58	174.8	1.0	170.8	Open Cylinder
10	4	2.55	.42	163.2	1.18	172.3	--	--	Lost C gage data
10	5	2.55	.38	162.4	1.40	173.7	.58	166.0	
10	6	2.55	.32	160.9	1.22	172.5	--	--	Lost C gage data
10	6	2.55Y	.34	161.4	1.14	171.9	.76	168.4	Yielding Baffles
10	6(1 Perf.)	2.55	.42	163.2	1.08	171.5	.60	166.3	Aft Chamber Perforated
10	6	3.0	.35	161.6	1.20	172.4	.78	168.6	
10	18	None	.68	167.4	1.66	175.2	1.0	170.8	Open Cylinder

*$db = 20 LOG_{10} \frac{P}{2.9008 \times 10^{-9}}$

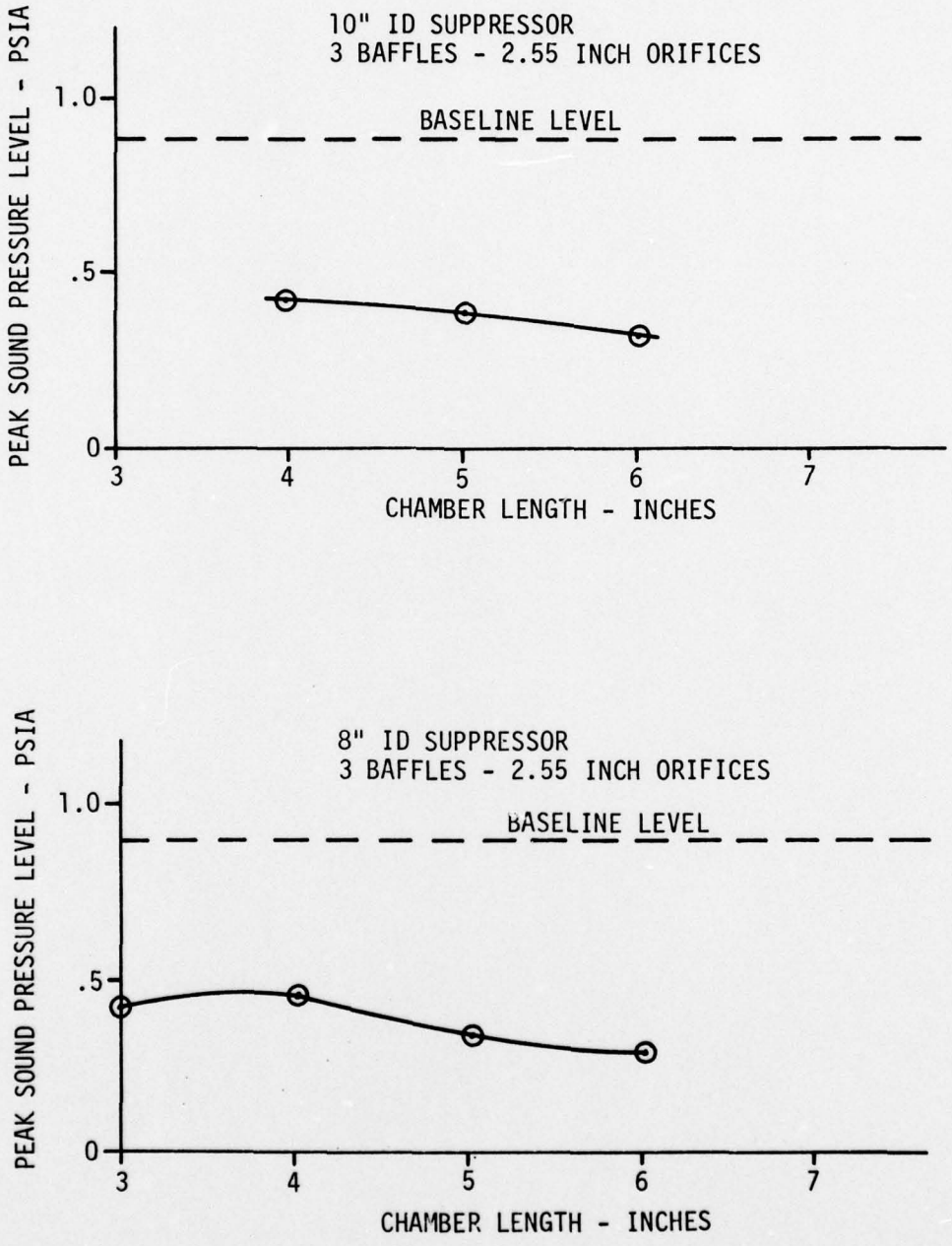

FIGURE 3-11. NOISE SUPPRESSOR CAPABILITIES AT THE A GAGE POSITION

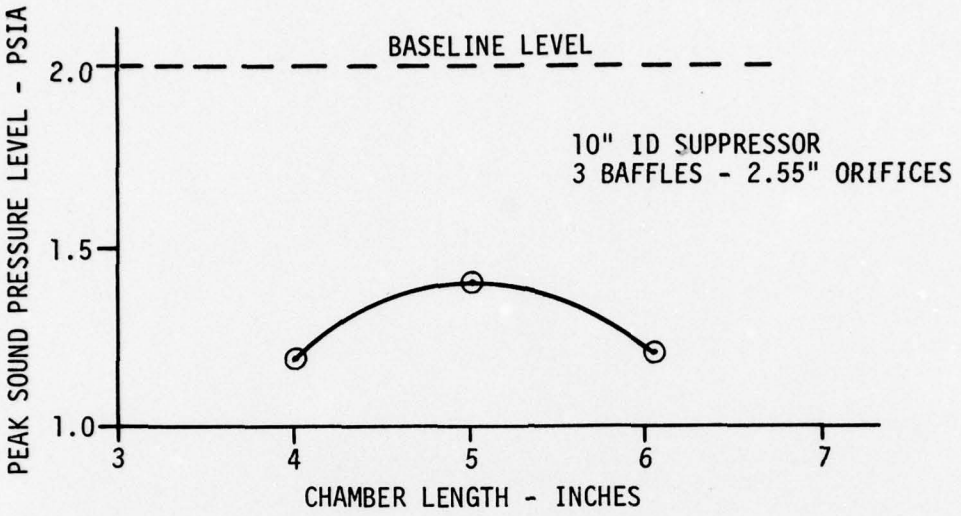

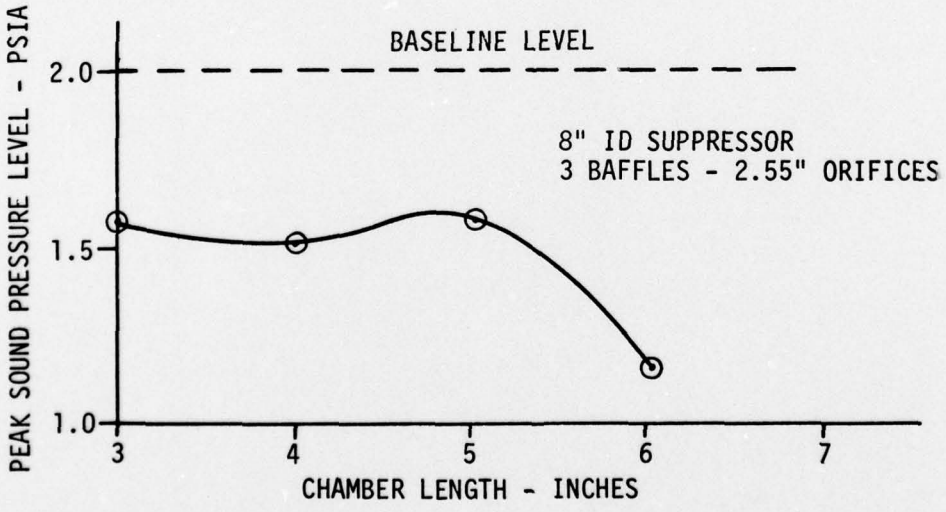

FIGURE 3-12. NOISE SUPPRESSOR CAPABILITIES AT THE B GAGE POSITION

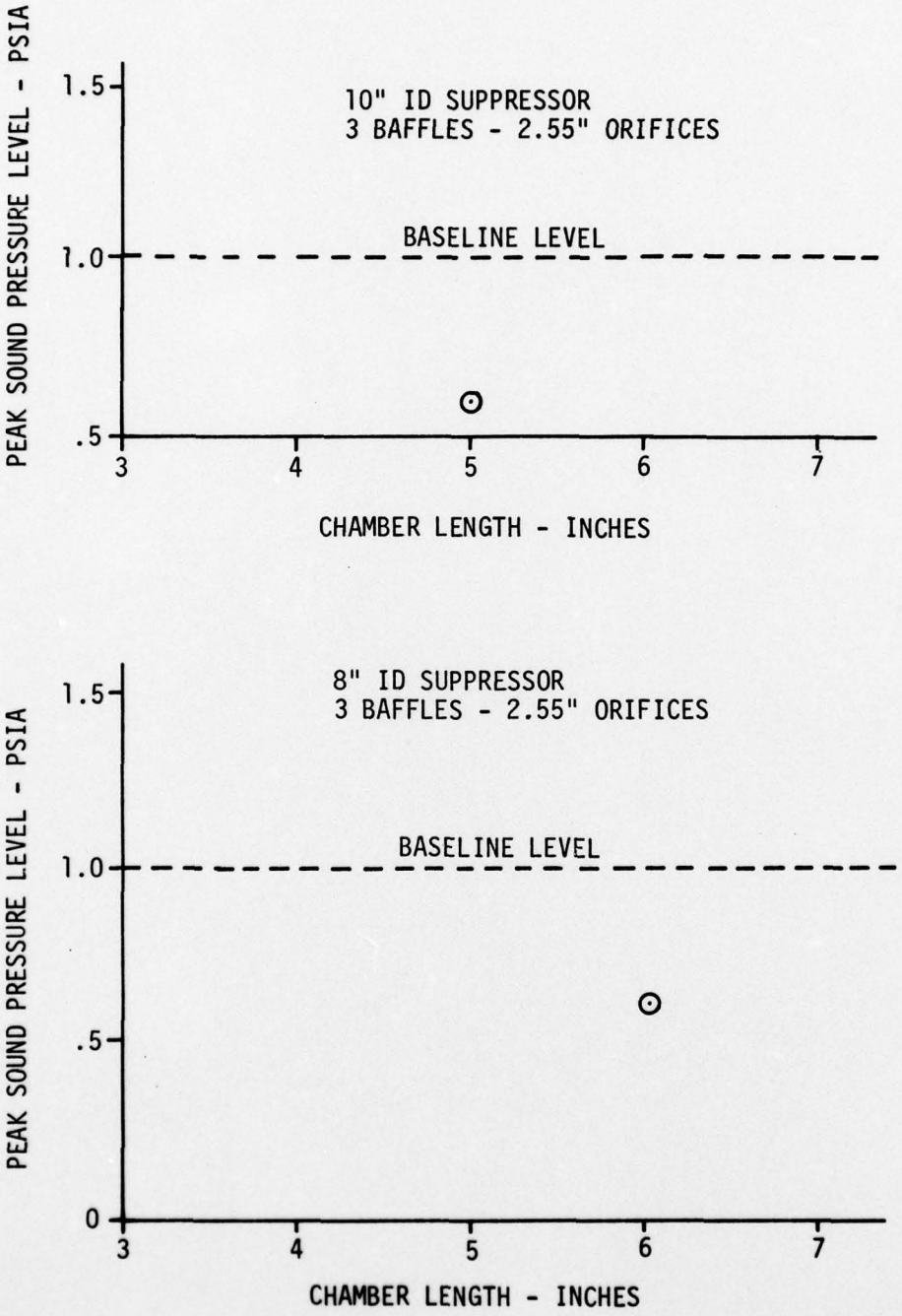

FIGURE 3-13. NOISE SUPPRESSOR CAPABILITIES AT THE C GAGE POSITION

3.3.1 (Continued)

the suppressor can be determined. In general the suppressors reduced the peak noise at all three gage positions. Specifically, the 8 inch suppressor with three six-inch chambers, reduced the sound pressure levels at all three gage positions as follows: A gage position from .88 psia to .28 psia; B gage position from 2.0 psia to 1.16 psia; C gage position from .996 psia to .62 psia.

The data on the A gage position, Figure 3-11, show that increasing chamber length between baffles will improve the capability of both the 8 and 10 inch suppressors. Similar data for the B gage position, Figure 3-12, show the same trend for the 8 inch suppressor. The B gage for the 10 inch suppressor show that chamber lengths above and below 5 inches make the suppressor more effective. Data for the C gage position, Figure 3-13, were lost due to an instrument failure for all chamber lengths except the 6 inch for the 8 inch suppressor and the 5 inch chambers for the 10 inch suppressor.

The baffle concept used in designing the suppressors was verified by determining the effect of the baffles, the effect of orifice size in the baffles and the effect of baffle rigidity. The data presented in Figures 3-14 show that the capability of the 8 and 10 inch suppressor is increased at all gage positions by adding baffles. The open cylinder provides some shielding to the A and B gage position but is no better than the unsuppressed baseline at the C gage position.

When the size of the orifice used in the baffles was varied, the capability of the suppressors was relatively unaffected as shown in Figure 3-15. The differences in the data for the two baffle orifice sizes are well within the motor to motor variations expected for the M-72 motor.

The 1/4" thick rigid baffles with the 2.55" orifice size were replaced with .060" thick baffles to determine the suppressor capability with baffles that would yield and absorb pressure wave energy as well as reflect the

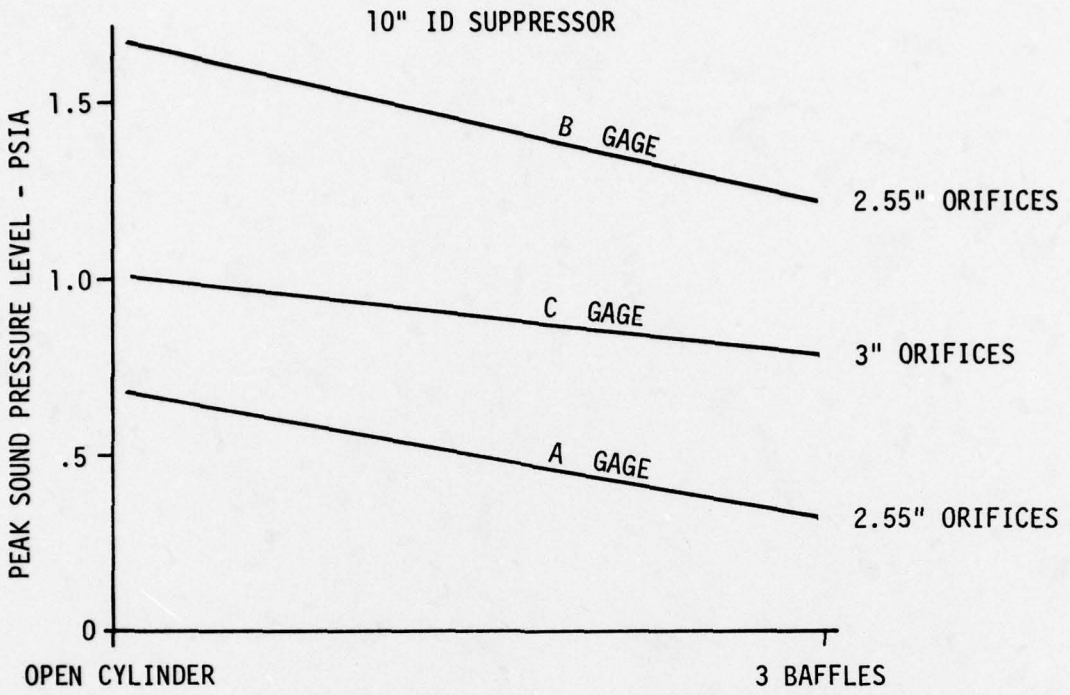

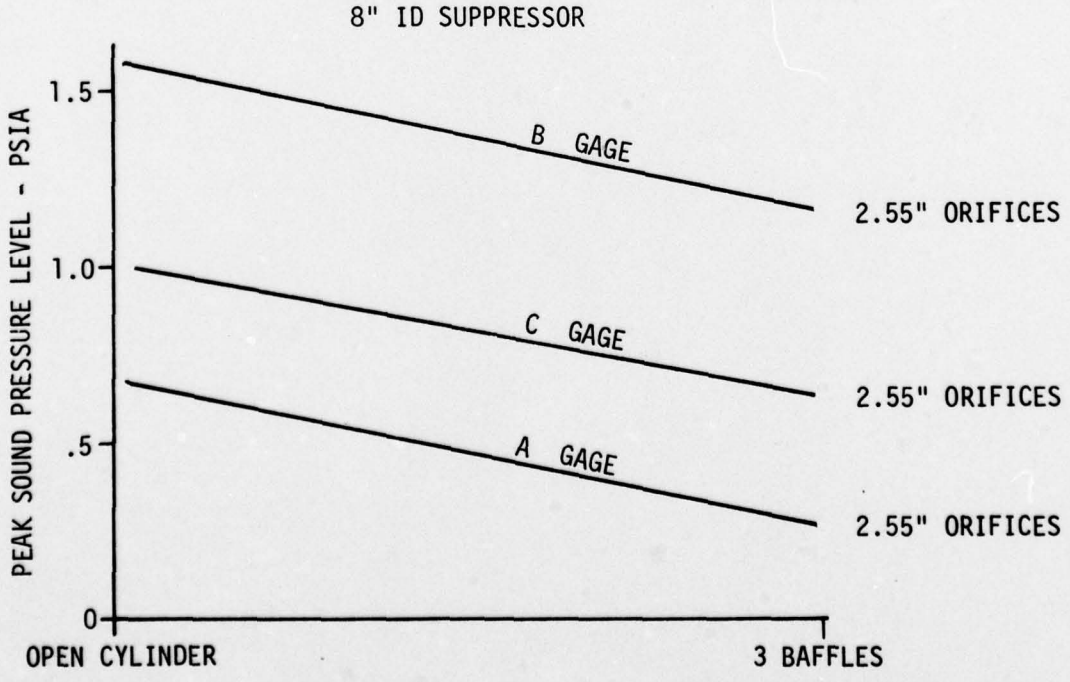

FIGURE 3-14. NOISE SUPPRESSOR CAPABILITY WITH AND WITHOUT BAFFLES

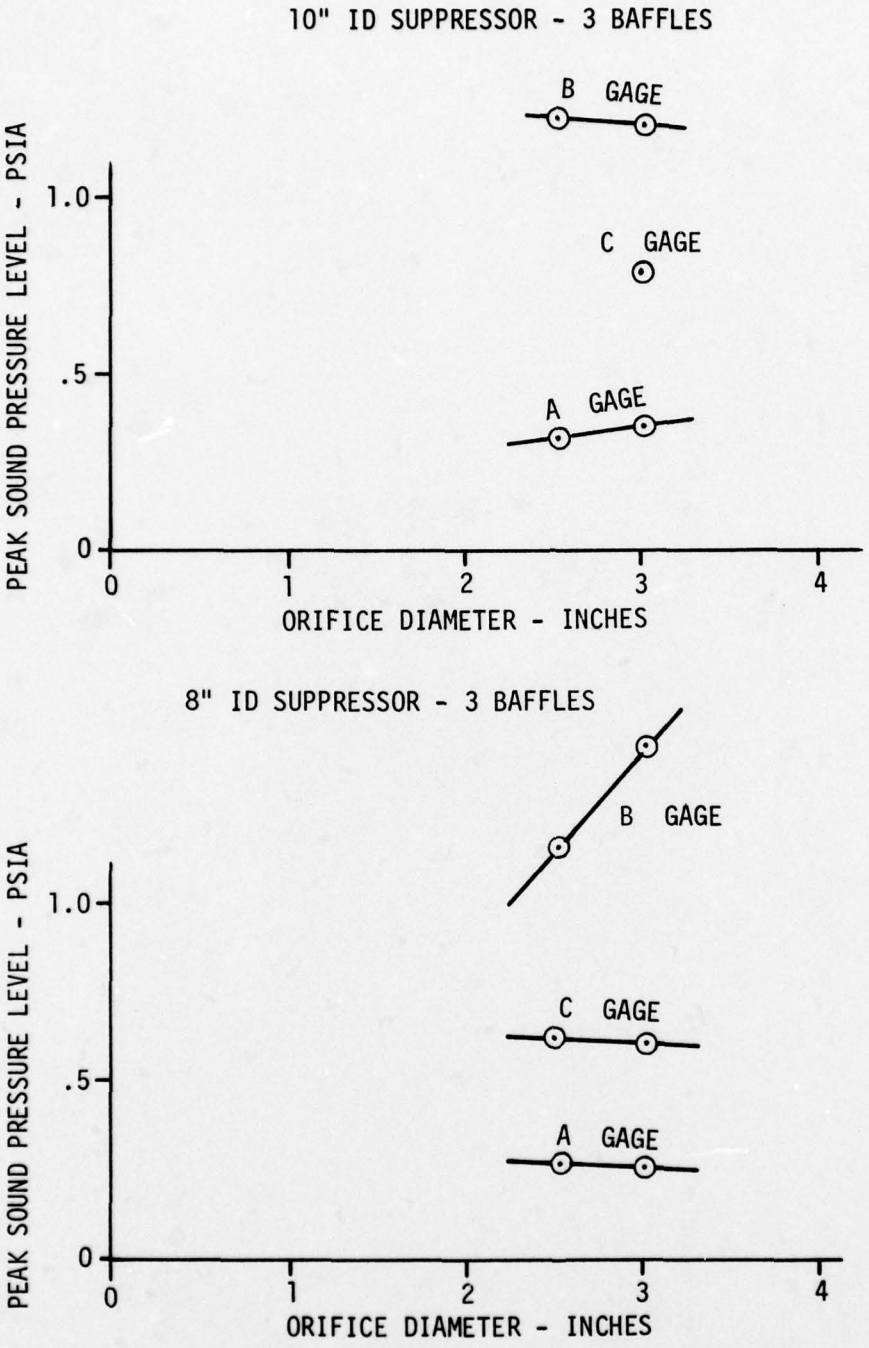

FIGURE 3-15. NOISE SUPPRESSOR CAPABILITY WITH VARYING ORIFICE DIAMETERS

3.3.1 (Continued)

pressure wave. The results of this test, Figure 3-16, show that the suppressor capability was unaffected by allowing the baffles to yield. This performance characteristic is a strong indication that if yielding baffles are used in the field weight system, suppressor performance will not be degraded.

To investigate the effect of perforations in the chamber walls, the 8 and 10 inch suppressors were tested with a perforated segment installed in the aft chamber. This chamber was perforated with 24 - 1/2 inch diameter holes. Both the 8 and 10 inch suppressor capability was reduced at the A gage position as shown in Figure 3-17. The effectiveness at the B and C gage position appear to increase for the 8 inch suppressor and decrease at the B gage position for the 10 inch suppressor.

Each baffled suppressor tested was instrumented for internal chamber pressure. Pressure transducers located in each chamber between the baffles recorded the pressure-time history. A typical oscillograph trace of these data is shown in Figure 3-10. The maximum pressure recorded in each chamber during the test is tabulated in Table 3-II. These data are

TABLE 3-II. NOISE SUPPRESSOR MAXIMUM CHAMBER PRESSURES

SUPPRESSOR CONFIGURATION (3 CHAMBERS)			CHAMBER PRESSURE - PSIA			COMMENTS
INSIDE DIAMETER INCHES	CHAMBER LENGTH INCHES	ORIFICE SIZE INCHES	LOCATION			
			FORWARD	CENTER	AFT	
8	3	2.55	50	215	285	
8	4	2.55	50	175	195	
8	5	2.55	60	135	340	
8	6	2.55	110	465	--	Aft Chamber Unreadable
8	6	2.55Y	115	430	320	
8	6(1 Perf.)	2.55	105	715	200	
8	6	3.0	155	450	215	
10	4	2.55	240	295	995	
10	5	2.55	70	70	160	
10	6	2.55	70	80	220	
10	6	2.55Y	75	175	165	
10	6(1 Perf.)	2.55	--	195	125	Fwd Chamber Unreadable
10	6	3.0	80	140	140	

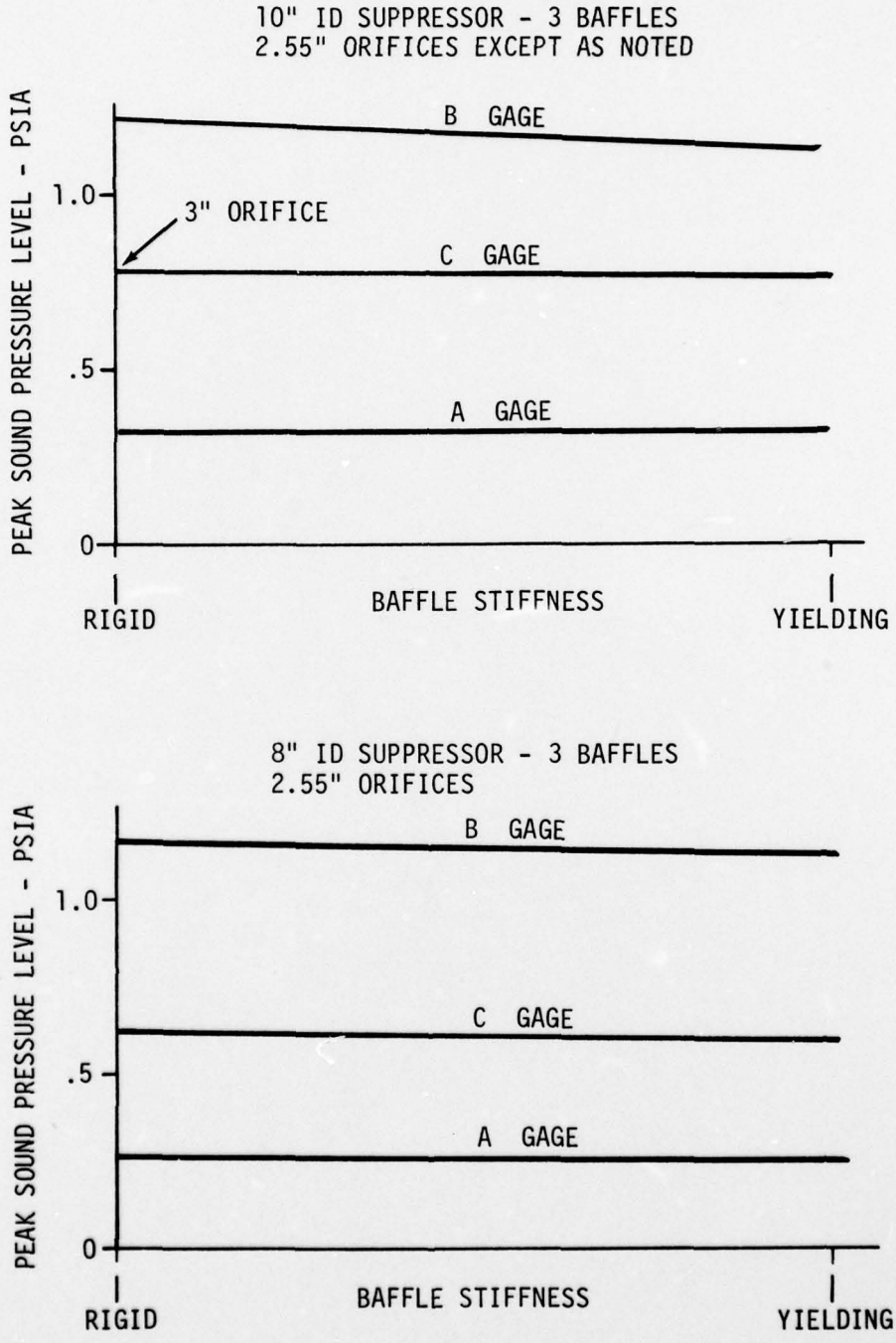

FIGURE 3-16. NOISE SUPPRESSOR CAPABILITY WITH YIELDING BAFFLES

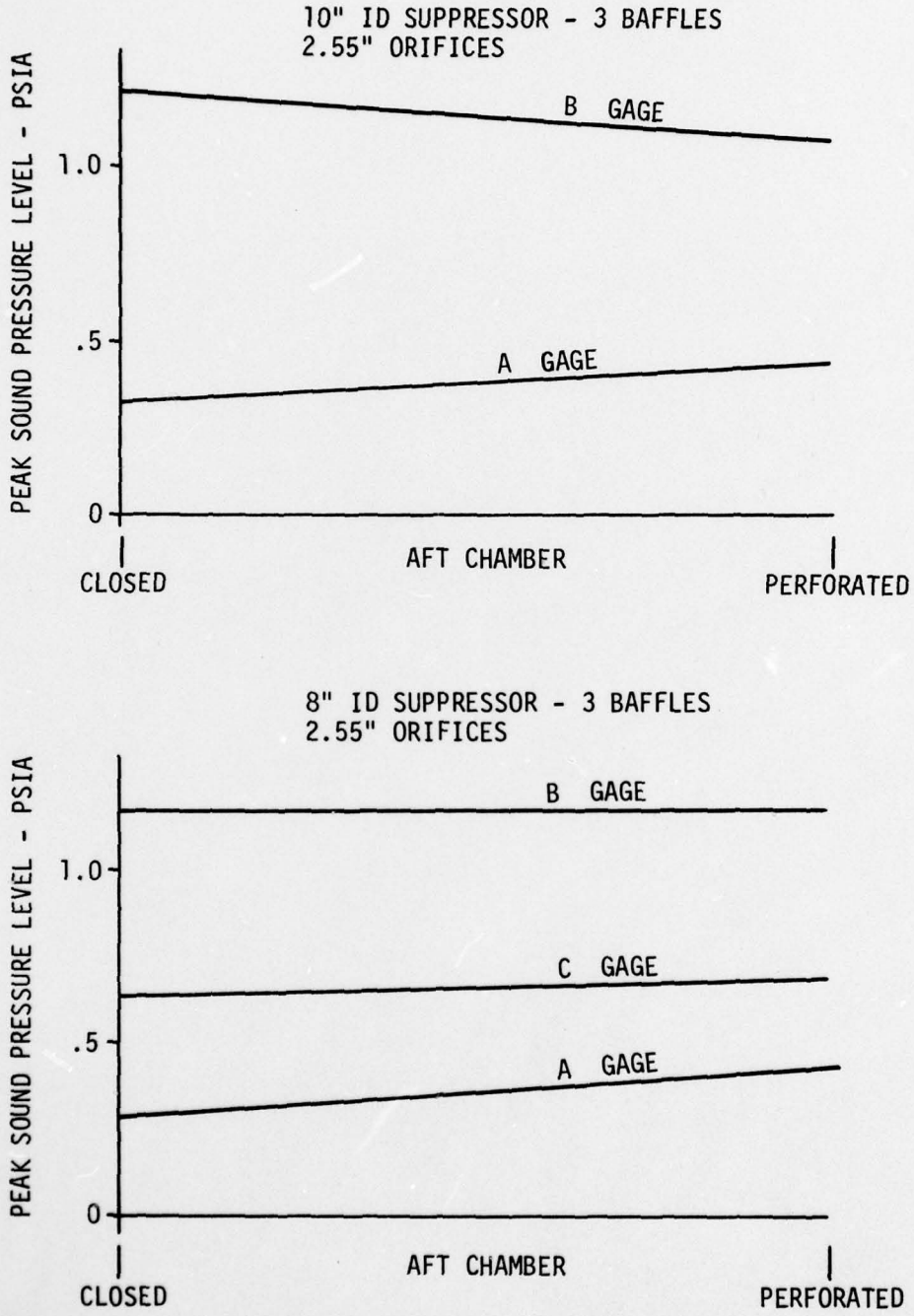

FIGURE 3-17. NOISE SUPPRESSOR CAPABILITIES WITH PERFORATIONS

3.3.1 (Continued)

representative of the maximum pressure that will be seen in the respective chambers. In general the quieter 10 inch suppressors have the lower chamber pressures. The quieter 8 inch suppressors tend to have higher chamber pressures when compared to the 10 inch suppressors.

3.3.2 Noise Suppressor Effect On Motor Performance and Recoil

The test fixture used to test the noise suppressor, Figure 3-8, was designed with dual load cells for measuring both thrust and recoil. The basic principal used to resolve these two forces is shown in Figure 3-18. Motor thrust can be measured directly with the thrust load cell. The force measured by the recoil load cell will be the thrust if the recoil forces are zero. Any forces imparted to the fixture other than thrust will change the force measured by the recoil load cell. The difference between the force measured by the thrust load cell and the force measured by the recoil load cell can be interpreted as recoil forces.

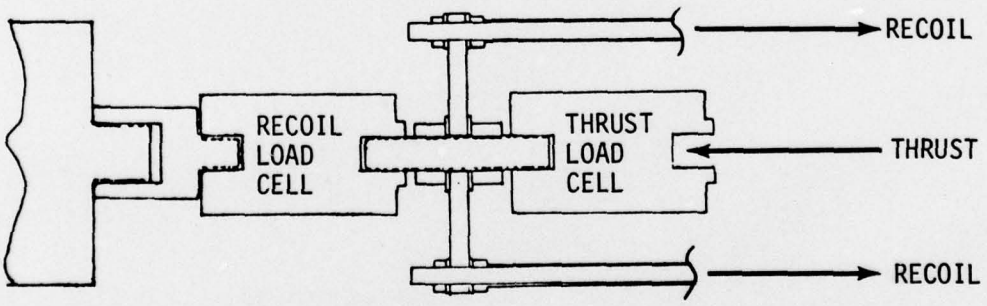

FIGURE 3-18. THRUST AND RECOIL RESOLUTION SCHEMATIC

3.3.2 (Continued)

The two load cells were selected and calibrated so that each would give the same thrust trace when measuring the same force. The initial tests with the fixture were used to verify this simularity. Typical thrust traces for the load cell for the case where recoil is zero are shown in Figure 3-19. The two thrust traces are not absolutely identical but do agree with the accuracy of two separate load cells.

When the suppressors were attached to the test fixture as shown in Figure 3-8, the measured data from the thrust and recoil load cells were not of the same characteristics as shown in Figure 3-19. A comparison of the thrust load cell measured data with and without the suppressors installed is shown in Figure 3-20. The measured data with the suppressors installed indicate that there is some vibrational motion in the fixture that causes cyclic bending moments that are measured in the load cell as cyclic thrust. A comparison of the force measured by the recoil load cell with and without the suppressors installed is shown in Figure 3-21. The effect of the vibrational motion is more apparent in the recoil load cell since it supports the test fixture on each end of the load cell. The larger bending moments imparted to the recoil load cell are measured as cyclic forces.

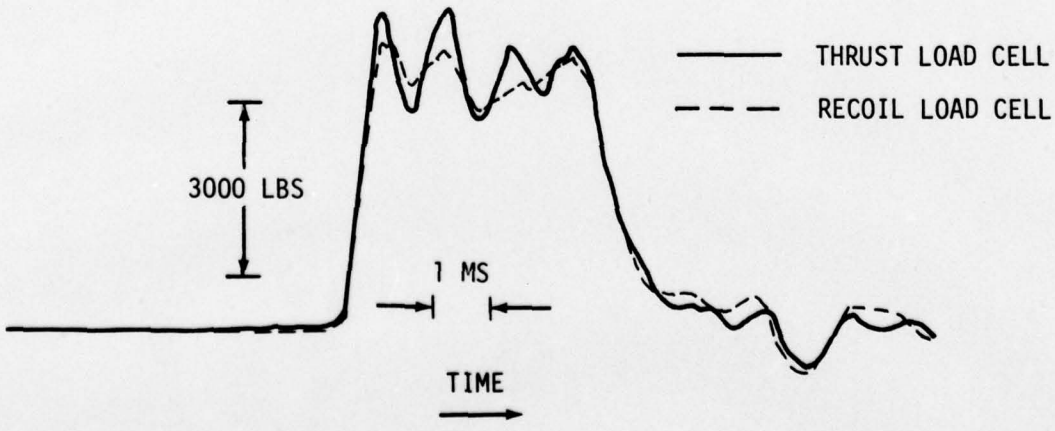

FIGURE 3-19. THRUST AND RECOIL LOAD CELL SIMILARITY

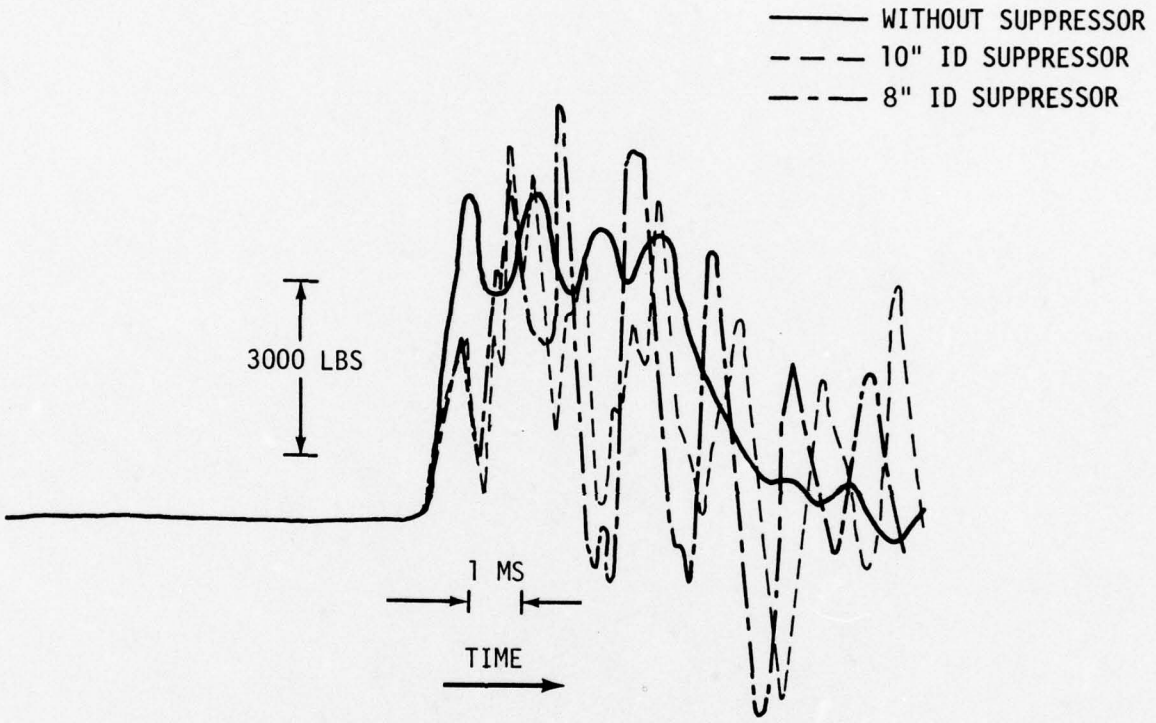

FIGURE 3-20. TYPICAL THRUST LOAD CELL MEASUREMENT

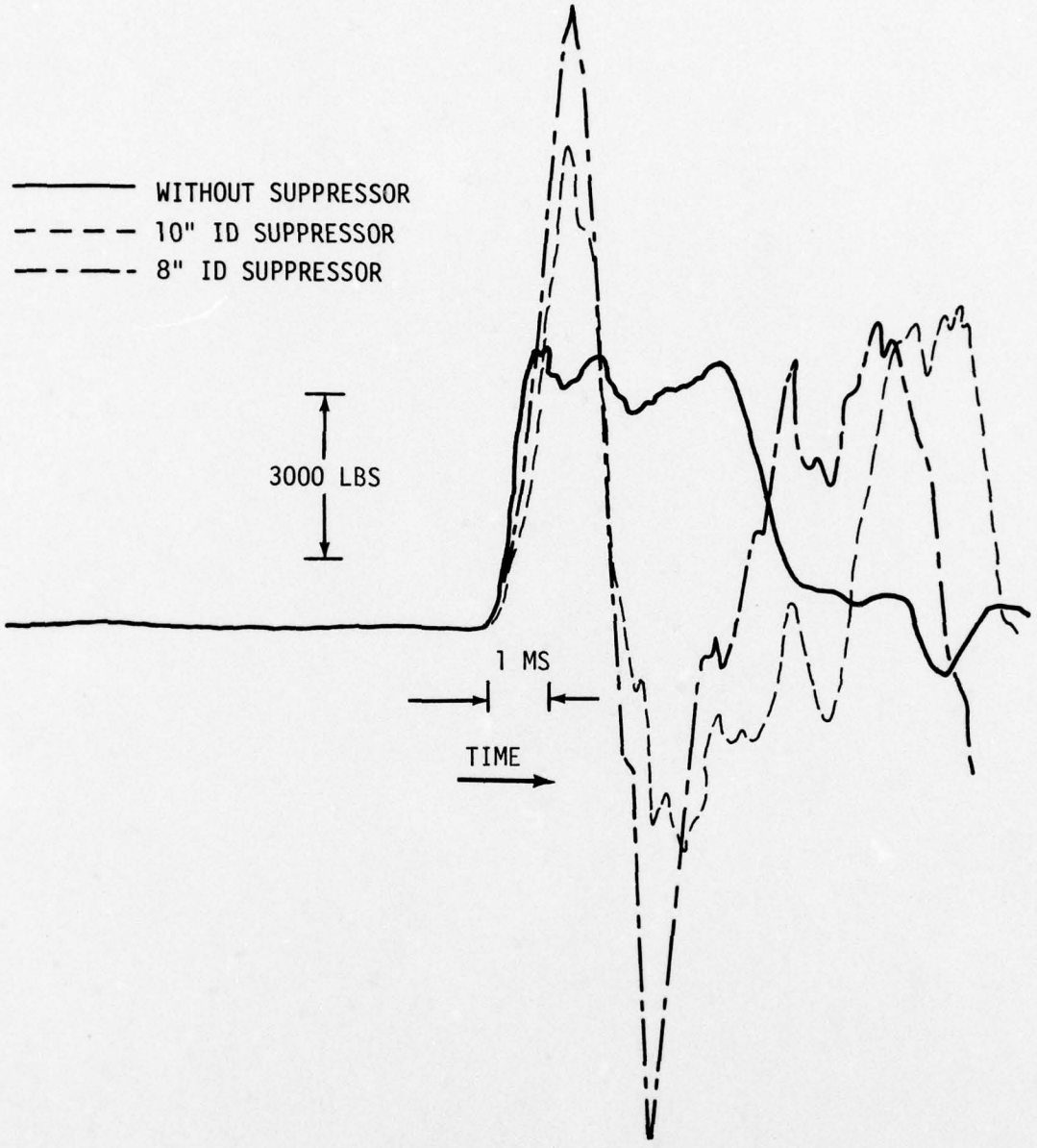

FIGURE 3-21. TYPICAL RECOIL LOAD CELL MEASUREMENT

3.3.2 (Continued)

The overall test fixture installation was flexible due to the size of the threaded connectors in the load cells. With this inherent flexibility, the motion in the test fixture could have been initiated by several possible areas of misalignment such as: the load cells and the motor, the load cells and the test fixture, the test fixture and the suppressors and non-parallel baffles in the suppressors.

The motion initiated bending moments imparted to the load cells is superimposed on the axial forces measured by the thrust and recoil load cells. In effect, the load cells are not measuring forces for which they can be calibrated to measure. No acceptable method was developed to separate the bending moments and the axial forces since the load cells cannot be calibrated to resolve both bending moments and axial forces. The existing test fixture has both alignment and load cell problems and will require complete redesign to determine the effect of the suppressor on motor performance and launcher recoil. It is recommended that a pendulum type test fixture be designed and fabricated for further tests with the suppressor.

4.0 PEAK NOISE ANALYTICAL/EXPERIMENTAL ANALYSIS

In order to approach rationally the noise suppression problem it is necessary to understand the character of the sound field produced by the rocket firing and the mechanism of energy absorption by a properly designed noise suppressor. To this end, an analysis of the generated sound field based on explosion theory was carried out. At the same time a theoretical analysis upon tested noise suppressors has been performed. The most important parameter in analyzing the sound field theory is the energy released by the explosion. This parameter could not be directly measured but was estimated from acoustic measurements made in the far field. To quantify the role of the baffles, a physical mechanism was postulated; it is based on the attenuation of shock waves as it propagates through the constriction formed by orifices in the baffle.

4.1 EXPLOSION THEORY

When the nozzle closure is released from the rocket motor a strong pressure wave is emitted from the motor. This problem is geometrically very difficult to analyze in any simple manner. However, it has a certain analogy to a strong explosion. Several solutions to the strong explosion problem are known (see Sedov, Ref. 2) and therefore it will be useful to make a comparison with the predictions of these theories. Although the geometry of the closure release from the rocket motor (and noise suppressor) is very complicated, it will be assumed initially that the wave motion is spherical. This is approximately true until the projectile overtakes the initial pressure wave. This is illustrated in Figures 3-1 and 4-1 taken from Reference 3.

Consider the problem of a strong explosion at $t = 0$ in a gas at rest from a point of symmetry ($r = 0$) with an instantaneous release of energy E_0. The ambient atmosphere has density ρ_1, pressure p_1, and specific heat ratio γ. Assuming adiabatic perfect gas processes the spherical explosion will be a function of the following dependent and independent quantities:

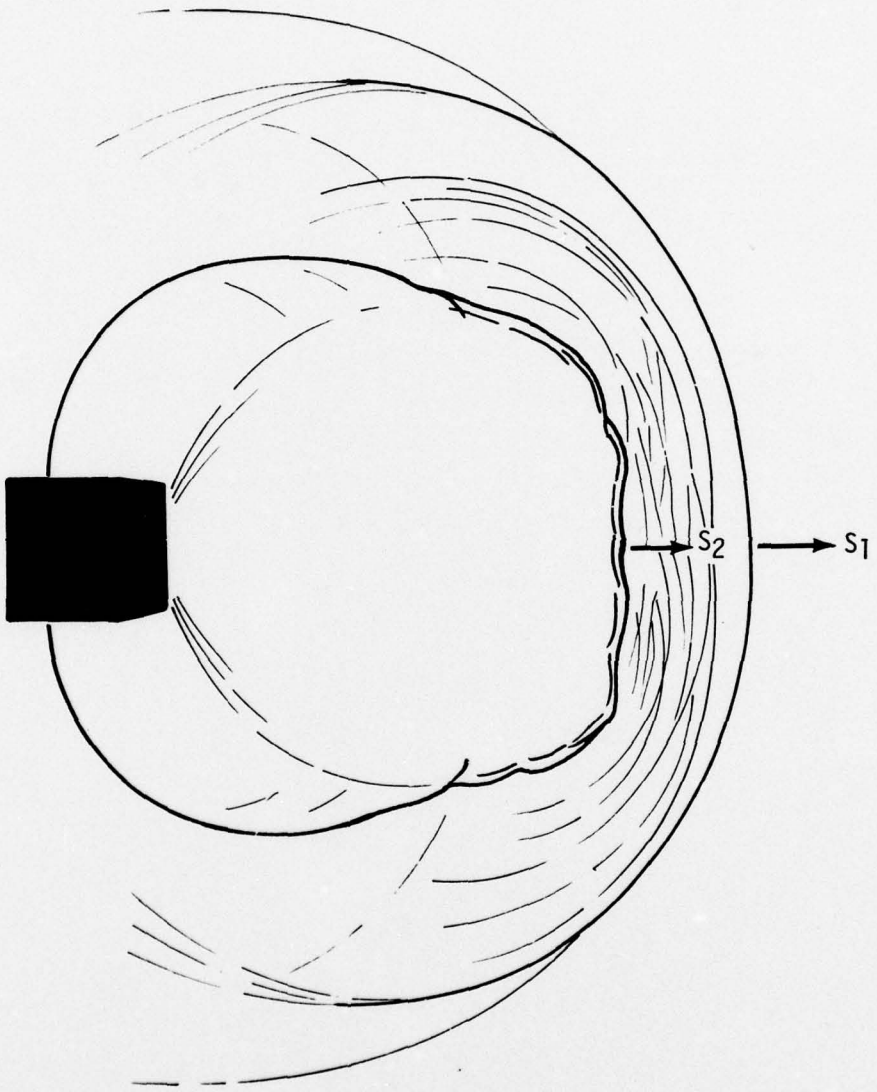

FIGURE 4-1. SHOCK WAVE PRODUCED 250 μSEC AFTER FIRING A .30 CALIBER BULLET (FROM REFERENCE 2)

4.1 (Continued)

$$p_1,\ \rho_1,\ E_o,\ r,\ t,\ \gamma$$

Dimensional analysis then shows that all the independent nondimensional quantities can only depend on three nondimensional parameters:

$$\gamma;\ \bar{R} = \frac{r}{\left[\frac{E_o}{\rho_1}\right]^{1/5} t^{2/5}}\ ;\ \tau = \frac{P_1^{5/6} t}{E_o^{1/3} \rho_1^{1/2}}$$

$\bar{R}$ and τ are nondimensional variables for the radius and the time. γ is the specific heat ratio and relates directly to the properties of the medium.

A strong spherical shockwave is formed and moves radially from the point of the explosion. An abrupt change of properties takes place across this shock. The parameter τ enters because of the conditions that must be met at the shock.

If E_o is very large then the motion becomes independent of P_1, and P_1 can be taken to be zero. In this case τ is no longer a relevant parameter in the problem and $\bar{R}$ is the only remaining parameter. In this case neither a characteristic length nor a characteristic time exist and the motion is self-similar. The position of the shockwave, $\bar{R}$ is determined by the constant value $\bar{R}^*$ of the parameter $\bar{R}$. $\bar{R}^*$ has been determined from a complete solution to the problem and, for $\gamma = 1.4$ (air), is given by Thompson (Ref. 4), $\bar{R}^* = 1.033$. Therefore, at the shock location

$$\frac{R}{\left[\frac{E_o}{\rho_1}\right]^{1/5} t^{2/5}} = 1.033 = \bar{R}^*$$

4.1 (Continued)

This theory can be checked by plotting 5/2 log R vs. log t. If this theory is applicable then all the points would be on a straight line. However, the shock location, R, would have to be determined for many times.

The present instrumentation measured the time of arrival of the shock at two downstream locations (B and C gages). Therefore, it was more meaningful to use the equation to determine E_o (for measured R and t).

$$E_o = \frac{\rho \cdot R^5}{(1.033)^5} \frac{1}{t^2}$$

If the theory was applicable then E_o would be the same from the two gage measurements.

The gage locations were well known and the times for the arrival of the shockwaves at the gages could be determined within 1/10 ms but there was great uncertainty in the determination of the initiation of the energy release. This was estimated crudely from the rocket motor chamber pressure measurement. Nevertheless, all of the tests with and without the suppressor indicated that the time to reach the gages was approximately constant for all of the tests. The results are summarized in the table below.

Sound Pressure Level Gage	R (ft.)	$\bar{t}$ (sec.)	E_o (ft lb)
B	4.64	3.8×10^{-3}	2.9×10^5
C	9.28	7.6×10^{-3}	2.3×10^6

Because E_o is not constant from the two measurements, and is also unrealistically large, it can be assumed that this strong shock solution is not applicable to the present problem and the pressure p_1 (and parameter τ) cannot be ignored. Self-similarity of the problem is now lost.

4.1 (Continued)

When the parameters E_o, P_1, and ρ_1 are all necessary to describe the problem then a characteristic length and a characteristic time can be defined. Note that τ can be written as

$$\tau = \frac{t}{t_o}$$

is a characteristic time. Using this time in $\overline{R}$ gives

$$\overline{R} = \frac{r}{r_o}$$

where

$$r_o = (E_o/P_1)^{1/3}$$

is a characteristic distance. Notice that r_o and t_o can be determined only after E_o has been determined, assuming that the ambient conditions (p_1, ρ_1) are known.

The energy release, E_o, associated with the expulsion of the nozzle closure can be estimated from the pressure-time history by using an acoustic approximation. The energy density in an acoustic field is given by

$$\varepsilon = \frac{1}{2} \rho_1 \left(u^2 + \frac{p^2}{\rho_1^2 a_1^2}\right)$$

where ρ_1 and a_1 are undisturbed values of the density and sound speed, p is the acoustic pressure, and u is the particle velocity. Assuming spherical symmetry the total energy in the acoustic field is

$$E_o = 4\pi \int_0^R \varepsilon(r)\, r^2\, dr$$

where R is the location of the initial wavefront. Furthermore, it may be assumed that the pressure and particle velocity are in phase and are

4.1 (Continued)

related by, $\rho_1 a_1$, characteristic impedance of the medium - $u = p/\rho_1 a_1$

Thus

$$\varepsilon = \frac{p^2}{\rho_1 a_1}$$

and

$$E_o = 4\pi \int_0^R \frac{p^2}{\rho_1 a_1} r^2 \, dr$$

This integral can be changed to an integration over time at a fixed radial location R_o by assuming that the wavefront is moving at the speed of sound, $dR = a_1 \, dt$. Then

$$E_o = 4\pi R_o^2 \int_{T_1}^{T_2} \frac{p^2}{\rho_1 a_1} \, dt$$

Only the contribution of the initial pressure pulse was used to estimate the energy release and this was approximated by a triangular wave form as illustrated below.

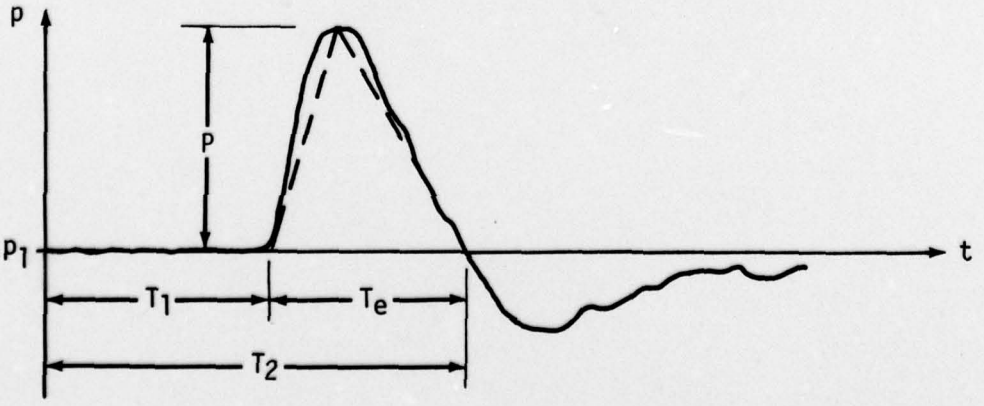

4.1 (Continued)

Then

$$J = \int_{T_1}^{T_2} \frac{p^2}{\rho_1 a_1} dt \approx \frac{p^2 T_c}{3 \rho_1 a_1}$$

and

$$E_o = 4\pi R_o^2 J$$

This use of only the initial positive waveform obviously underestimates the energy flux since there is considerable energy contained in the field after the first zero crossing. However, the evaluation of this contribution would require numerical integration with a decision as to when to terminate the integral and would very likely contain a contribution from reflected waves.

4.2 ANALYTICAL/THEORETICAL COMPARISON

The procedure described in paragraph 4.1 was used to estimate the energy release, E_o, based on gage measurements at positions B and C where such measurements were available. Ideally, the two calculations should give the same result; although the approximations that have been made would be better at position C, which is further from the source. Figure 4-2 shows a comparison between the estimated energy obtained from these two gage measurements. Although the two measurements agree fairly well (at least there is not the order of magnitude difference encountered in self-similar blast wave theory) the C gage usually yields a larger value of the energy release then the measurement at position B. This is primarily due to broadening of the initial pressure pulse duration, T_e, caused by the wavefront traveling faster than the speed of sound. Such effects are not accounted for in an acoustic approximation.

4.2 (Continued)

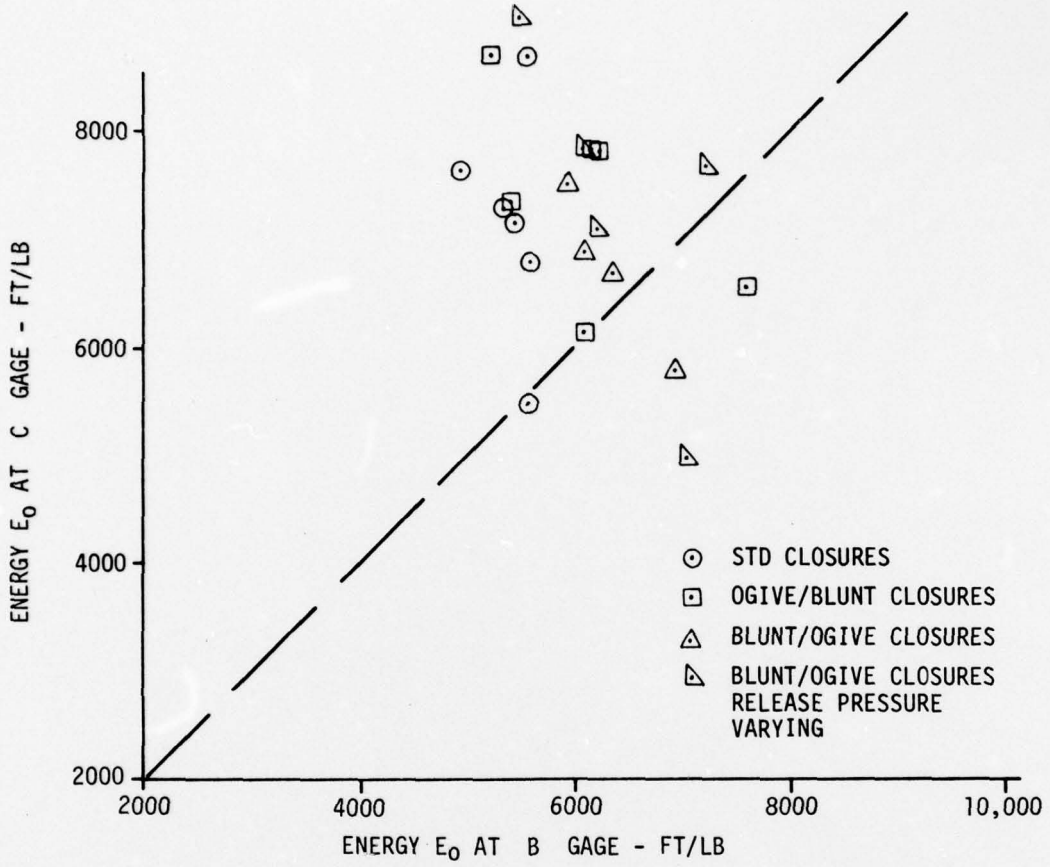

FIGURE 4-2. COMPARISON OF ENERGY E_o AS COMPUTED FROM B AND C GAGES

With this estimate of the sound energy released by the motor firing, an attempt was made to correlate the peak pressure with the dimensionless distance

$$\overline{R} = \frac{r}{r_o} = \frac{r\, p_1^{1/3}}{E_o^{1/3}}$$

The differences in the energies calculated from the two gages make little difference in the evaluation of $\overline{R}$ due to the cube root extraction. Data from both B and C gages are plotted in Figure 4-3 against dimensionless

4.2 (Continued)

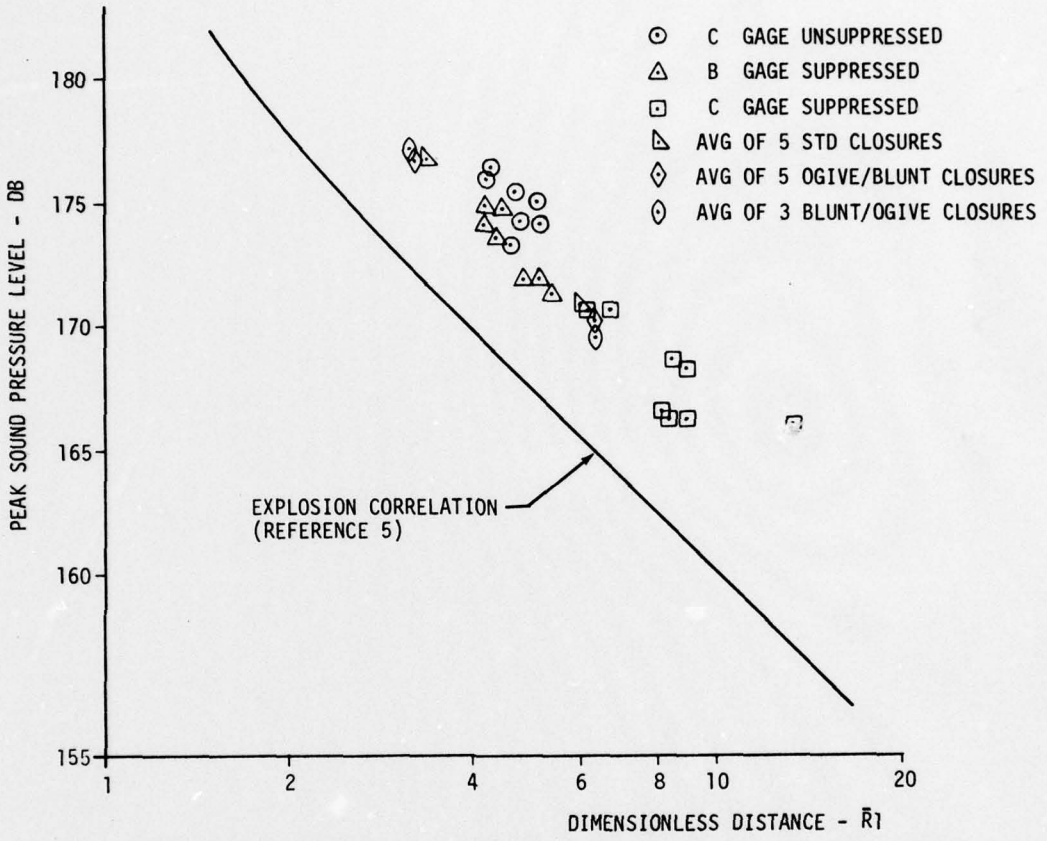

FIGURE 4-3. CORRELATION OF MICROPHONE DATA WITH EXPLOSION THEORY

distance $\bar{R}$. Data obtained from unsuppressed tests with different closure shapes and for different suppressor configurations are displayed on this graph. Also shown on this graph is a correlation for spherically symmetric explosion data taken from Chapter 6 of Explosions in Air, Reference 5.

The agreement between the pressure data and the point explosion correlation is considered to be reasonably good. The measured sound pressure data generally scatters about a line that is 5-6 dB above the correlation curve for point explosions. This discrepancy may be in part due to the underestimation of the energy release by considering only the energy contained in the initial triangular wave form. Increasing the energy values would decrease the values of $\bar{R}$ shifting the data points to the left.

4.2 (Continued)

A second possible source of the discrepancy is the lack of spherical symmetry of the sound field produced by the nozzle closure expulsion. This asymmetry in the absence of a suppressor is illustrated in Figure 4-4

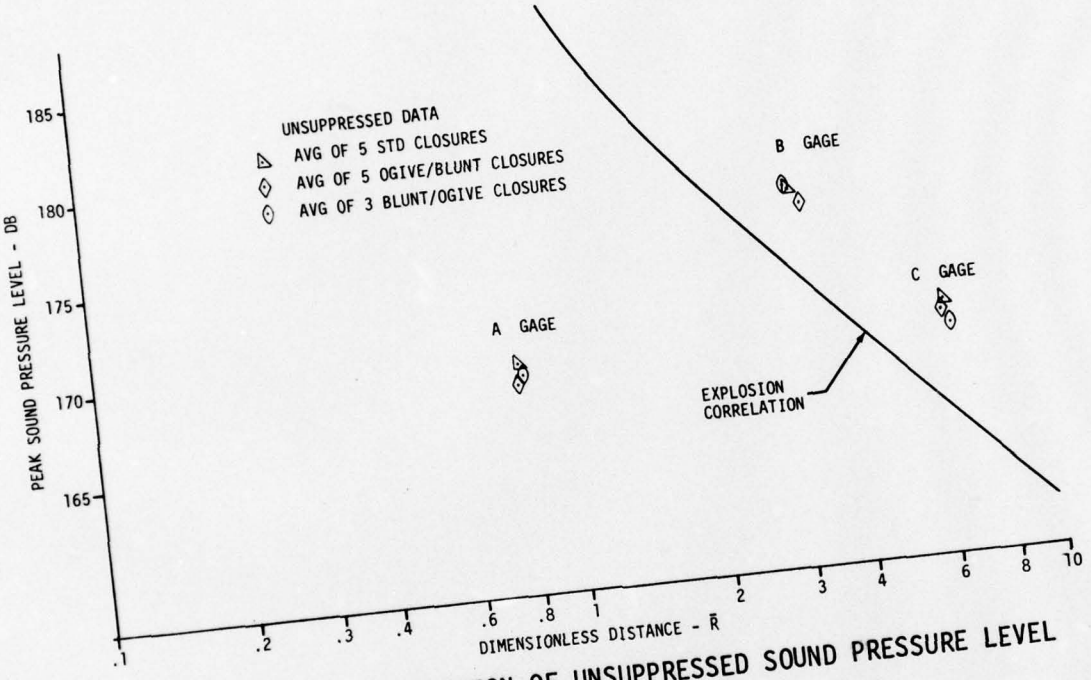

FIGURE 4-4. CORRELATION OF UNSUPPRESSED SOUND PRESSURE LEVEL

for where the peak sound pressure levels of all three gages are plotted against the non-dimensional distance $\bar{R}$. The energy used in the evaluation of $\bar{R}$ was calculated from sound pressure level data at the C gage. The gages at positions B and C are along a ray 45^{o} from the launcher axis while the A gage position is located along a ray 135^{o} from the axis. The measurements along the 45^{o} ray lie above the correlation for spherical waves while the data at 135^{o} is considerably below that correlation. It seems reasonable to suppose that, for the geometry under consideration, the location of the correlation curve shifts continuously with angular variation. Additional gage measurements would be required to determine the angular variation. An array of gages at a constant radial distance in the far field would allow a more accurate determination of the acoustic energy release as well.

4.2 (Continued)

Figure 4-5 shows the sound pressure level measured at the A gage as related to the energy release calculated from pressure data at the C gage. Data is presented in Figure 4-5 for the test series where the nozzle closure geometry was varied with no suppressor and the test series for different suppressor configurations.

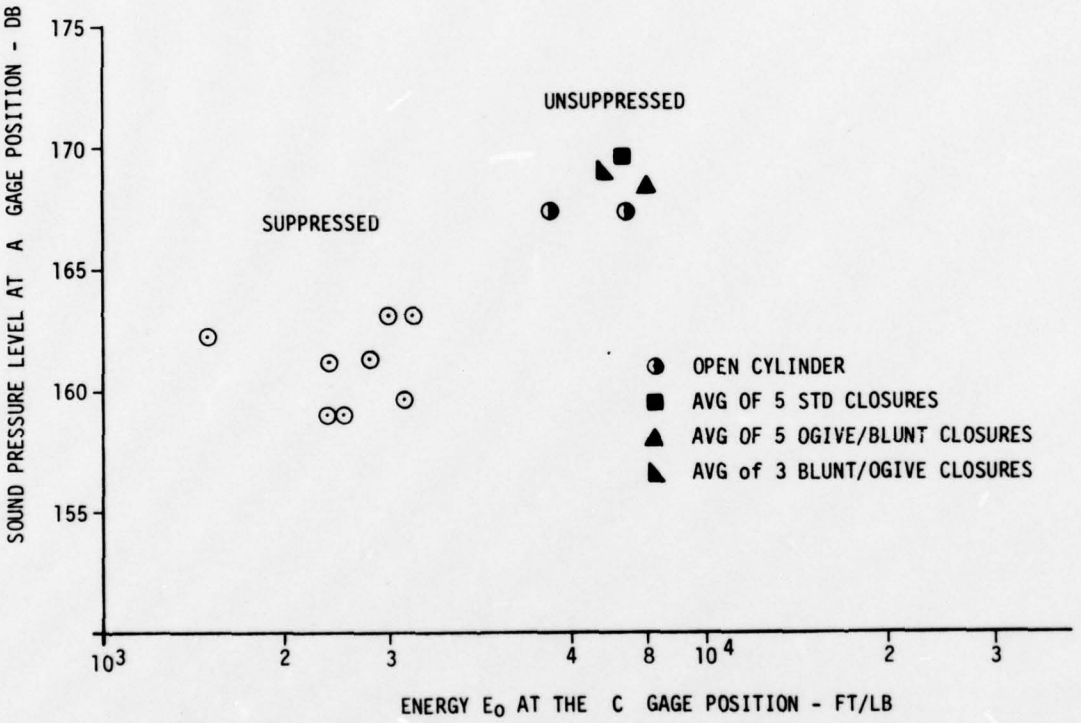

FIGURE 4-5. PEAK SOUND PRESSURE LEVEL AT A GAGE AS A FUNCTION OF ENERGY E_O

The average of several Ogive/Blunt and Blunt/Ogive tests show a slight reduction when compared to the average of 5 standard closure tests. It appears that any noise reduction achieved by the variation of plug shape alone tested would not be greater than 3 db.

4.2 (Continued)

Perhaps the most interesting feature of Figure 4-5 is the comparison of the data obtained with and without an attached suppressor. This comparison shows that the reduction in sound level perceived at the A gage position, by the addition of the suppressor is accompanied by a decrease in the acoustic energy as calculated from the C gage. Thus the suppressor is not just acting as a sound shield to create the acoustic shadow for the user but is also substantially *reducing* the acoustic energy that is escaping from the launcher. This conclusion is strengthened by the fact that the reduction obtained with only the suppressor with no baffles is only about 2 db. This reduction is probably primarily due to shielding. The internal baffles are essential for effective noise suppression and with them the acoustic energy escaping the launcher is substantially reduced.

4.3 QUANTITATIVE DISCUSSION OF THE SOUND ATTENTUATION DUE TO SUPPRESSORS

In this paragraph a physical explanation of the sound attenuation due to the provision of suppressors is developed and a quantitative estimate of the pressure reduction is presented. The analytical results compare rather favorably with the experimental results. The postulated physical mechanism also suggests that several future suppressors could have improved attenuation.

Let us focus our attention on the front surface of the pressure wave propagating through the suppressor. As a first approximation, we regard the pressure wave as a plane, normal shock. (Although, without the presence of the suppressor, the pressure wave may be regarded as spherical. Within the suppressor, we can neglect the curvature of the shock.) Figure 4-6 shows the shock front at its successive position as it propagates from left to right when it passes through a constriction imposed by the baffle orifice. No drastic change occurs to the shock strength until its front propagates beyond the constriction; then, owing to the sudden enlargement of the area, the shock strength becomes weaker to satisfy the requirement of mass conservation. This attenuation of the shock caused by the area change is considered to be the key mechanism of sound suppression.

4.3 (Continued)

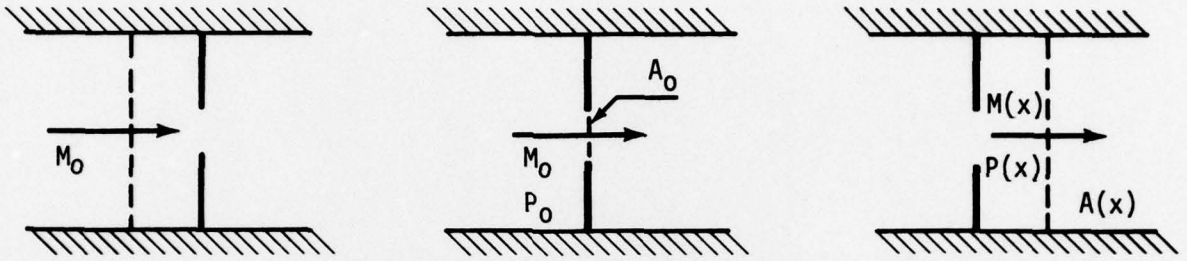

FIGURE 4-6. SHOCK PROPAGATION THROUGH BAFFLES

In order to quantify this effect, we apply the theory of shock propagation through a non-uniform duct developed by Whitham (Ref. 6). According to Whitham, if we designate the cross-sectional duct area, which is varying in the direction of propagation x, as A(x) and the Mach number of the moving shock as M(x), A(x) and M(x) are related by the following differential relationship:

$$\frac{M}{M^2 - 1} \lambda(M) \frac{dM}{dx} + \frac{1}{A} \frac{dA}{dx} = 0, \qquad (1)$$

where

$$\lambda(M) = \left(1 + \frac{2}{\lambda + 1} \frac{1 - \mu^2}{\mu}\right) \left(1 + 2\mu + \frac{1}{M^2}\right),$$

4.3 (Continued)

and

$$\mu^2 = \frac{(\gamma - 1) M^2 + 2}{2 \gamma M^2 - (\gamma - 1)} ,$$

and γ is the ratio of the specific heats. Although λ is a function of Mach number M, λ varies little over wide range of Mach number as one can see from the following limiting values:

for $M \to 1$, $\lambda \to 4$

$M \to \infty$, $\lambda \to 5.074$ (for $\gamma = 1.4$).

Thus for all practical purposes, one may regard λ as essentially constant and can integrate (1) to obtain

$$\frac{M^2(x) - 1}{M_0^2 - 1} = \left[\frac{A_0}{A(x)}\right]^{2/\lambda} , \qquad (2)$$

where the suffix 0 denotes the reference point taken at the orifice (Figure 4-6). When we express the pressure just behind the moving shock before and after passing the restriction as p_o and $p(x)$, respectively (Figure 4-6), its ratio may be obtained from the normal shock relationship and the condition that the pressure just ahead of the moving shock always remain constant (and equal to atmospheric pressure). This leads to

$$\frac{p(x)}{p_o} = \frac{2\gamma M^2(x) - (\gamma - 1)}{2\gamma M_0^2 - (\gamma - 1)} . \qquad (3)$$

Thus the sound attenuation, in decibels, due to the shock passage through the constriction is simply given by

$$db = 20 \log \frac{p(x)}{p_o}$$

4.3 (Continued)

$$db = 20 \log \frac{2\gamma \left(\frac{A_\sigma}{A(x)}\right)^{2/\lambda} (M_0^2 - 1) + 1 - (\gamma - 1)}{2\gamma M_0^2 - (\gamma - 1)} \qquad (4)$$

For the suppressor of 10" inner diameter and a baffle with a 2.55" orifice diameter,

$$A(x) = \left(\frac{10}{2}\right)^2 \pi = 78.34 \text{ sq. in.}$$

$$A_0 = \left(\frac{2.55}{2}\right) \pi = 5.11 \text{ sq. in.}$$

According to the data available, the Mach number of the escaping air at the time of firing is equal to 3. The initial Mach number of the moving shock, M_0, may be obtained from this value and the shock formulae and obtained to be

$$M_0 = 3.8.$$

From these, (4) yields

$$\Delta db = 7 \text{ db.}$$

This is the sound attenuation due to the passage of the shock through one baffle. The effect of the additional baffles can be estimated in a similar fashion, although it should be noted, from the outset, that as the shock travels further downstream, the above idealization of the shock as planar, normal shock becomes less and less accurate. Nevertheless, if we repeat the above procedure to include the second constriction, the combined effect of the first and the second constriction is estimated to be

$$\Delta db = 13 \text{ db.}$$

4.3 (Continued)

Because of the aforementioned breakdown of the shock model, the actual reduction would be probably somewhat less than this value. (The effect of the third baffle cannot be estimated by the Whitham's theory, because, its being the last, it involves the shock expansion into unbounded space; its effectiveness in noise reduction is considered to be marginal and neglected in the present estimate). Collecting the above calculated results, the noise reduction due to the provision of the baffles is estimated to be

$$7 \text{ db} < \Delta\text{db} < 13 \text{ db. (Calculated)}$$

In spite of its rather crude approximation, this value appears to compare favorably with the experimental data; if we compare the unsuppressed data (Table 2-IV) with the suppressor data for 10" ID suppressor with 2.55" orifice (Table 3-I), Δdb is found to be

$$\Delta\text{db} = 169.7 - 160.9 = 8.6 \text{ db (Experimental)}$$

and this is close to the value estimated above. The multiple interaction between baffles and the sound attenuation should be studied in our next phase of investigation.

5.0 RECOMMENDATIONS

Based on the test and analyses performed as a part of the Rocket Motor Peak Noise Reduction Program the following recommendations are made.

1. The suppressor tests should be continued using the existing hardware to establish design parameters such as: (1) the optimum number of baffles, (2) the optimum chamber length between baffles, (3) the optimum orifice size and (4) the effectivity of the suppressor lined with sound absorbing material. Tests should be included to establish the combined effects of the noise suppressing closures, low closure release pressure and the suppressor configuration. These tests should be performed with the suppressor attached to a test fixture that is designed to accurately measure both rocket motor performance and launcher recoil. Instrumentation should be expanded to include (1) flow visualization of the pressure waves and the nozzle closure motion and (2) additional sound pressure level measurements in the near and far field to better define the pressure wave characteristics.

2. In view of the success of the shock propagation theory for explaining the sound attenuation in the baffled suppressor, the test data and results should be utilized to design prototype field weight suppressors. These suppressor designs should be based on the existing data and the design parameters established in the continued suppressor tests recommended in (1) above. The configurations should include new suppressor concepts that have surfaced during the tests and analyses conducted for this program such as that shown in Figure 1-5.

3. The test data and analysis techniques developed for the suppressor during tests with the M-72 motor should be used to design and fabricate suppressors for tests on other small rocket motor systems.

5.0 (Continued)

4. Pressure wave attenuation devices other than the baffled suppressor should be designed, fabricated and tested. These suppressors could take the form of an energy absorbing bag as shown in Figure 1-6.

APPENDIX A

DESIGN DRAWINGS

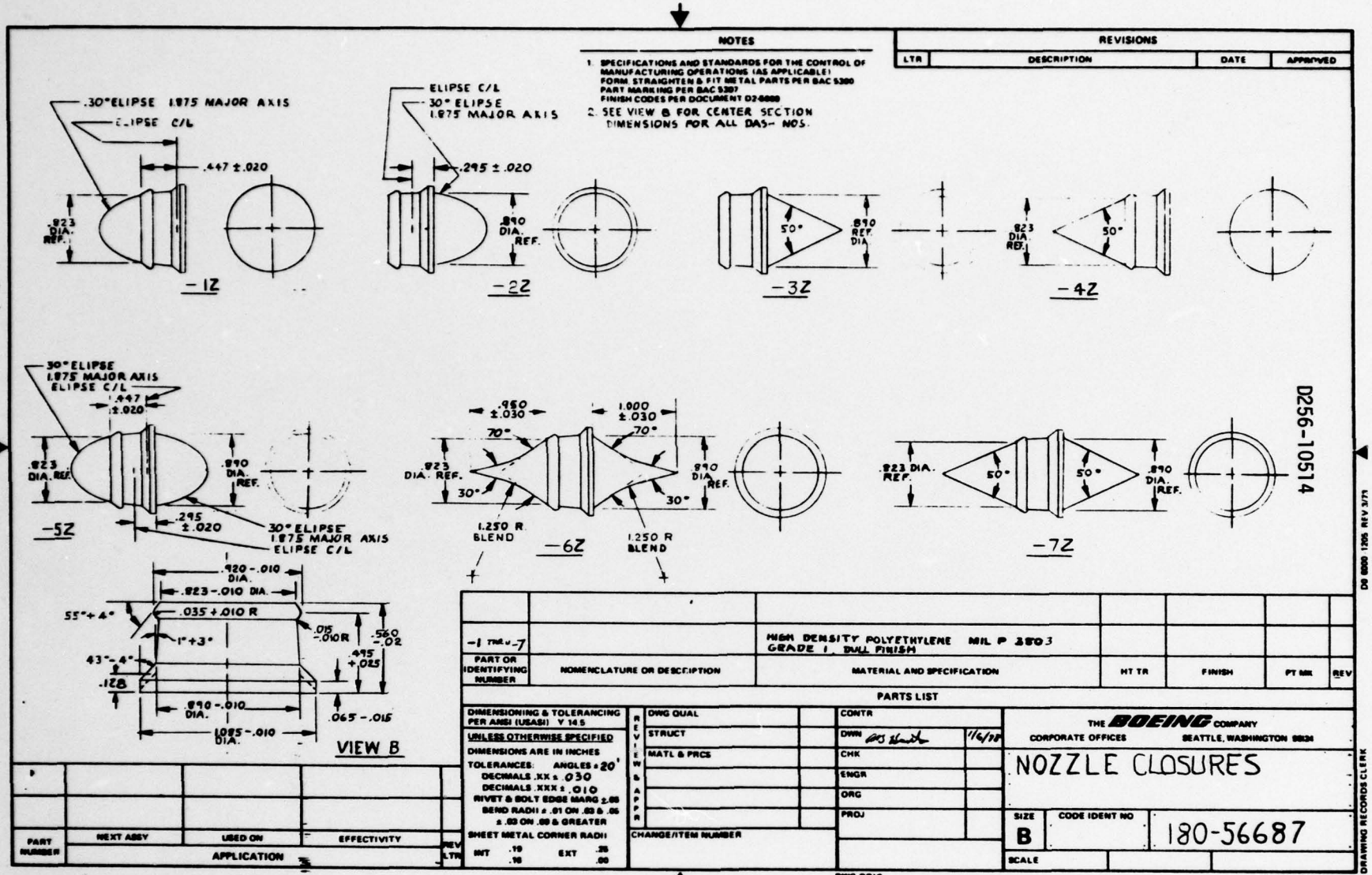

NOTES

1. SPECIFICATIONS AND STANDARDS FOR THE CONTROL OF MANUFACTURING OPERATIONS (AS APPLICABLE)
   FORM, STRAIGHTEN & FIT METAL PARTS PER BAC 5300
   PART MARKING PER BAC 5307
   FINISH CODES PER DOCUMENT D7-6000

REVISIONS			
LTR	DESCRIPTION	DATE	APPROVED

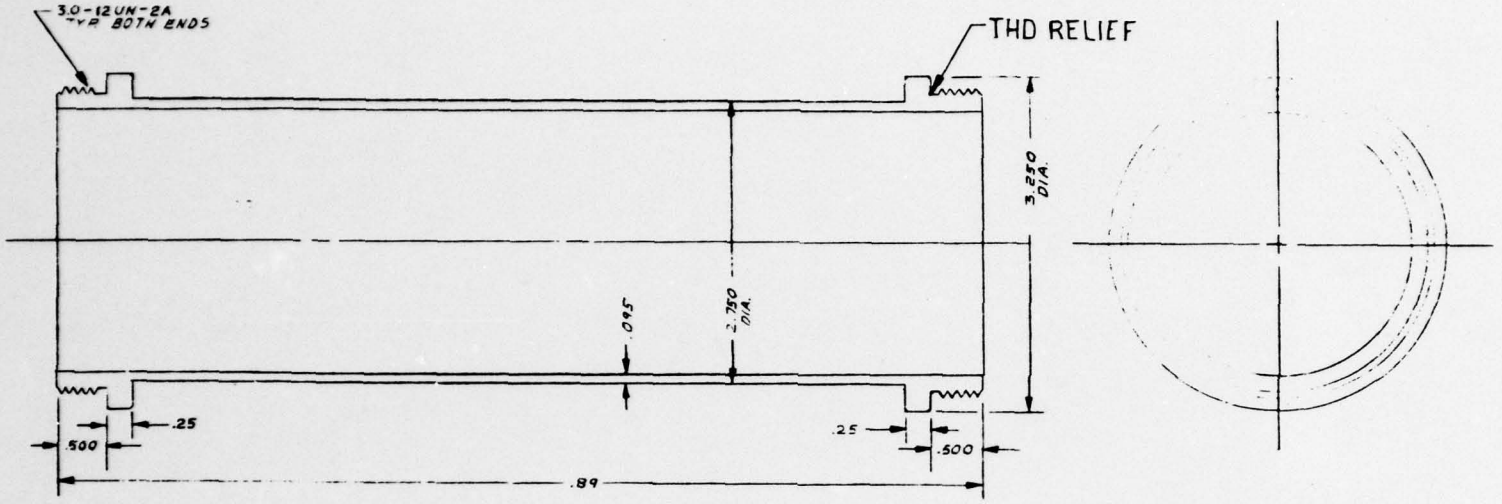

D256-10514

PART OR IDENTIFYING NUMBER	NOMENCLATURE OR DESCRIPTION	MATERIAL AND SPECIFICATION	HT TR	FINISH	PT MK	REV
	LAUNCH TUBE SIMULATOR	3/4 SS PLATE, 2.75 DIA X .095 WALL DOM SS TUBE				

PARTS LIST

PART NUMBER	NEXT ASSY	USED ON	EFFECTIVITY	REV LTR
		APPLICATION		

DIMENSIONING & TOLERANCING PER ANSI (USASI) Y 14.5

UNLESS OTHERWISE SPECIFIED
DIMENSIONS ARE IN INCHES
TOLERANCES: ANGLES ±
DECIMALS XX ± .030
DECIMALS XXX ± .010
RIVET & BOLT EDGE MARG ± .05
BEND RADII ± .01 ON .03 & .06
± .03 ON .09 & GREATER
SHEET METAL CORNER RADII
INT .19 .16 EXT .25 .00

REVIEW & APPR

DWG QUAL		
STRUCT		
MATL & PRCS		

CHANGE/ITEM NUMBER

CONTR		
DWN L.A.H	12/7/73	
CHK		
ENGR R.J.H	12/13/73	
ORG		
PROJ		

DWG DRIG BY (ORG) _____

THE BOEING COMPANY
CORPORATE OFFICES SEATTLE, WASHINGTON 98124

TEST FIXTURE - LAUNCH TUBE SIMULATOR

SIZE	CODE IDENT NO	
B	81205	180-56688
SCALE		

DRAWING RECORDS CLERK

DOD 6000 1705 REV 3/73

A-4

NOTES

1. SPECIFICATIONS AND STANDARDS FOR THE CONTROL OF MANUFACTURING OPERATIONS (AS APPLICABLE)
   FORM, STRAIGHTEN & FIT METAL PARTS PER BAC 5300
   PART MARKING PER BAC 5307
   FINISH CODES PER DOCUMENT D2-6000

REVISIONS			
LTR	DESCRIPTION	DATE	APPROVED

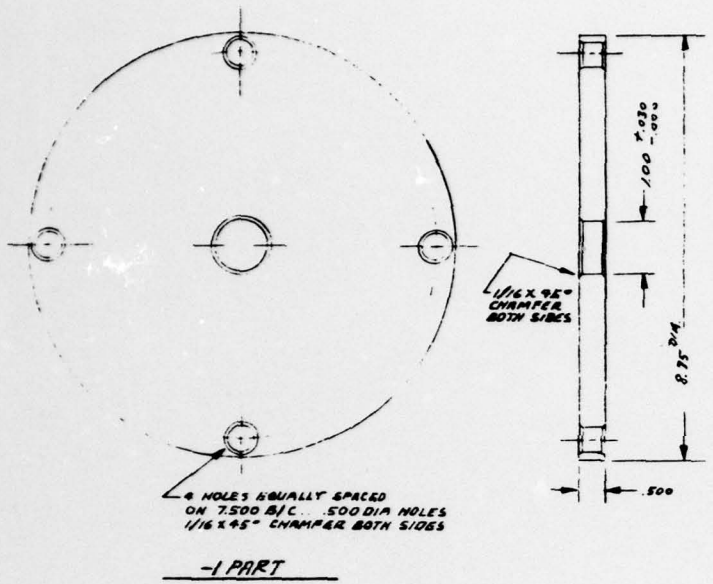

-1 PART

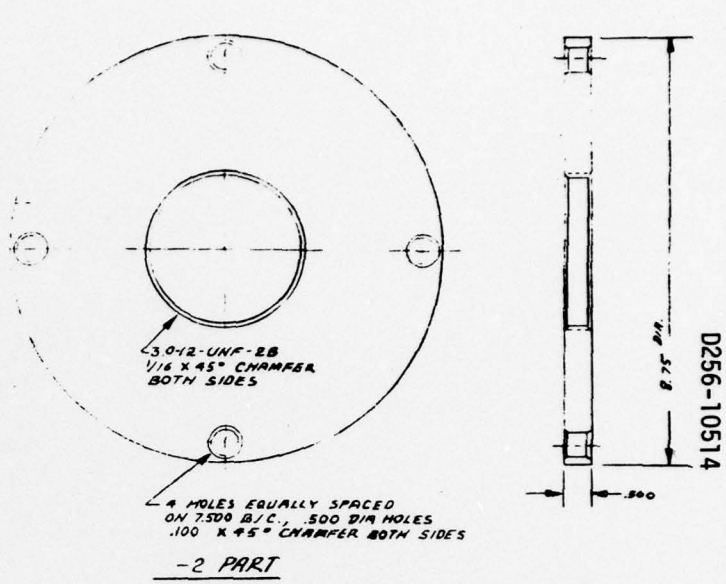

-2 PART

D256-10514

PART OR IDENTIFYING NUMBER	NOMENCLATURE OR DESCRIPTION	MATERIAL AND SPECIFICATION	HT TR	FINISH	PT MK	REV
-1	FORWARD SUPPORT FLA.	1/2 STEEL PLATE		BLACK OXIDE		
-2	AFT. SUPPORT FLA.	1/2 STEEL PLATE		BLACK OXIDE		

PARTS LIST

PART NUMBER	NEXT ASSY	USED ON	EFFECTIVITY	REV LTR
	APPLICATION			

DIMENSIONING & TOLERANCING PER ANSI (USASI) Y 14.5
UNLESS OTHERWISE SPECIFIED
DIMENSIONS ARE IN INCHES
TOLERANCES: ANGLES ± 20'
DECIMALS .XX ± .020
DECIMALS .XXX ± .010
RIVET & BOLT EDGE MARG ±.06
BEND RADII ± .01 ON .03 & .05
± .03 ON .09 & GREATER
SHEET METAL CORNER RADII
INT .19 .16 EXT .25 .60

REVIEW & APPR: DWG QUAL, STRUCT, MATL & PRCS

CHANGE/ITEM NUMBER

CONTR
DWN A.B. HUNTER 1/20/78
CHK
ENGR
ORG
PROJ

DWG ORIG BY (ORG)

THE BOEING COMPANY
CORPORATE OFFICES SEATTLE, WASHINGTON 98124

TEST FIXTURE - SUPPORT FLANGES

SIZE B | CODE IDENT NO 81205 | 180-56689

SCALE 1/2

DRAWING RECORDS CLERK

DD 6000 1205 REV 3/73

D256-10514

NOTES

1. SPECIFICATIONS AND STANDARDS FOR THE CONTROL OF MANUFACTURING OPERATIONS (AS APPLICABLE)
   FORM, STRAIGHTEN & FIT METAL PARTS PER BAC 5300
   PART MARKING PER BAC 5307
   FINISH CODES PER DOCUMENT D2-6000

REVISIONS			
LTR	DESCRIPTION	DATE	APPROVED

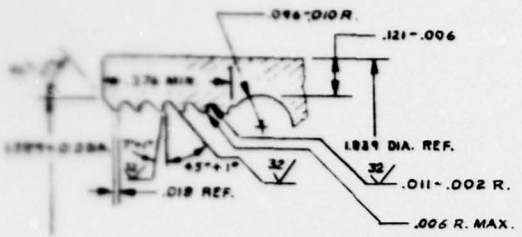

DETAIL A

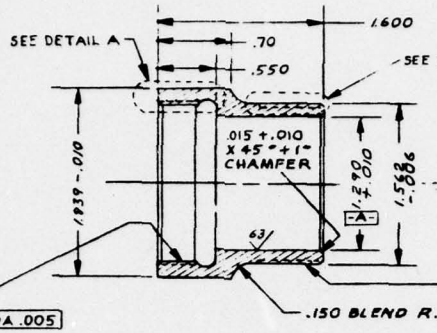

1.5785-16 BUTTRESS-2B
MAJOR DIA. 1.5730 MIN.
PITCH DIA. 1.5410+.0060 Ⓜ A .005
MINOR DIA. 1.5170+.0050

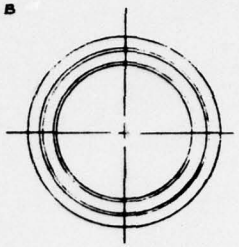

1.5785-16 BUTTRESS 2A
MAJOR DIA. 1.5620-.0060
PITCH DIA. 1.5370-.0050 Ⓜ A .005
MINOR DIA. 1.5050 MAX.

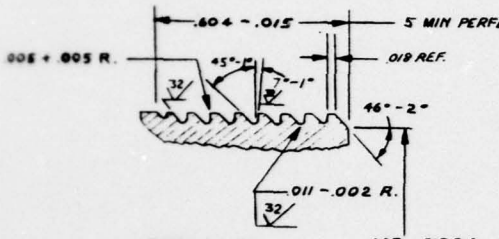

DETAIL B

PART OR IDENTIFYING NUMBER	NOMENCLATURE OR DESCRIPTION	MATERIAL AND SPECIFICATION	HT TR	FINISH	PT MK	REV
	MOTOR CASE EXTENSION	STAINLESS STEEL -				

PARTS LIST

PART NUMBER	NEXT ASSY	USED ON	EFFECTIVITY	REV LTR
	APPLICATION			

DIMENSIONING & TOLERANCING PER ANSI (USASI) Y 14.5
UNLESS OTHERWISE SPECIFIED
DIMENSIONS ARE IN INCHES
TOLERANCES: ANGLES ±
DECIMALS .XX ± .030
DECIMALS .XXX ± .010
RIVET & BOLT EDGE MARG ±.05
BEND RADII ± .01 ON .02 & .06
± .03 ON .09 & GREATER
SHEET METAL CORNER RADII
INT .19 .16 EXT .25 .00

REVIEW & APPR: DWG QUAL; STRUCT; MATL & PRCS
CHANGE/ITEM NUMBER

CONTR
DWN A.B. HUNTER 1/22/73
CHK
ENGR
ORG
PROJ
DWG ORIG BY (ORG)

THE BOEING COMPANY
CORPORATE OFFICES SEATTLE, WASHINGTON 98124

MOTOR CASE EXTENSION

SIZE	CODE IDENT NO	
B	81205	180-56690

SCALE

DRAWING BECOMES FIRM

A-6

NOTES

1. SPECIFICATIONS AND STANDARDS FOR THE CONTROL OF MANUFACTURING OPERATIONS (AS APPLICABLE)
   FORM, STRAIGHTEN & FIT METAL PARTS PER BAC 5300
   PART MARKING PER BAC 5307
   FINISH CODES PER DOCUMENT D2-6000

REVISIONS			
LTR	DESCRIPTION	DATE	APPROVED

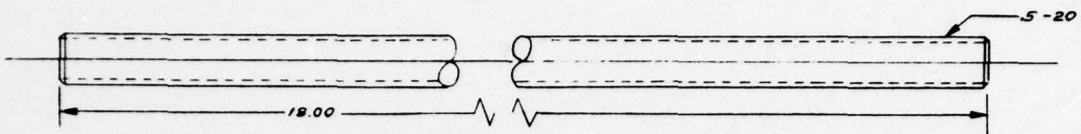

-1 PART

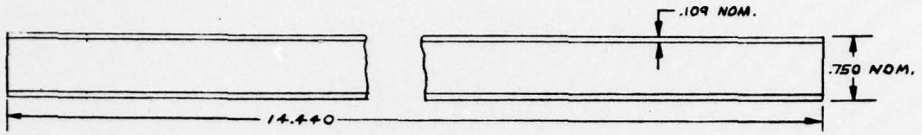

-2 PART

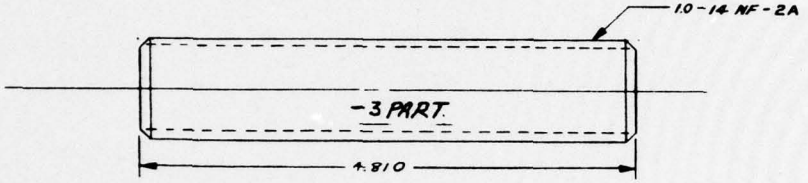

D256-10514

PART OR IDENTIFYING NUMBER	NOMENCLATURE OR DESCRIPTION	MATERIAL AND SPECIFICATION	HT TR	FINISH	PT MK	REV
-2	SPACER	M/S OR S/S DOM WELDED TUBING	—			
-1, -3	STUD.	MILD STEEL - THREADED ROD	—	CAD PLATE		

PARTS LIST

PART NUMBER	NEXT ASSY	USED ON	EFFECTIVITY	REV LTR

APPLICATION

DIMENSIONING & TOLERANCING PER ANSI (USASI) Y 14.5

UNLESS OTHERWISE SPECIFIED
DIMENSIONS ARE IN INCHES
TOLERANCES: ANGLES ±
DECIMALS .XX ± .030
DECIMALS .XXX ± .010
RIVET & BOLT EDGE MARG ±.06
BEND RADII ± .01 ON .03 & .06
± .03 ON .09 & GREATER
SHEET METAL CORNER RADII
INT .19 .16 EXT .25 .00

REVIEW & APPR

DWG QUAL		CONTR	
STRUCT		DWN	
MATL & PRCS		CHK	
		ENGR	
		ORG	
		PROJ	

CHANGE/ITEM NUMBER

DWG ORIG BY (ORG) _____

THE BOEING COMPANY
CORPORATE OFFICES SEATTLE, WASHINGTON 98124

TEST FIXTURE - SPACERS & STUDS.

SIZE	CODE IDENT NO	
B	81205	180-56691

SCALE

DRAWING RECORDS CLERK
DD 1 JAN 1205 REV 2/72 6000 DD

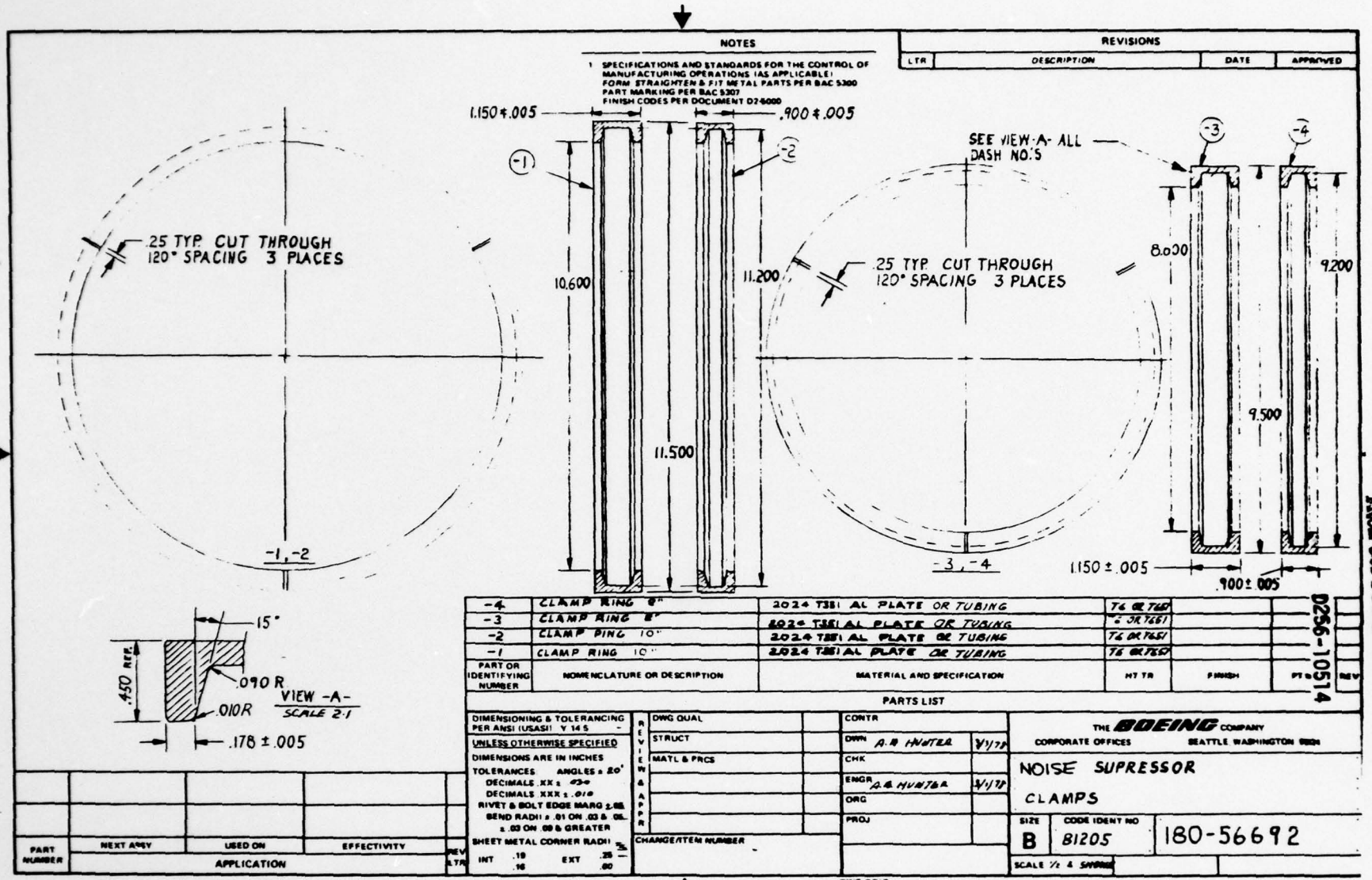

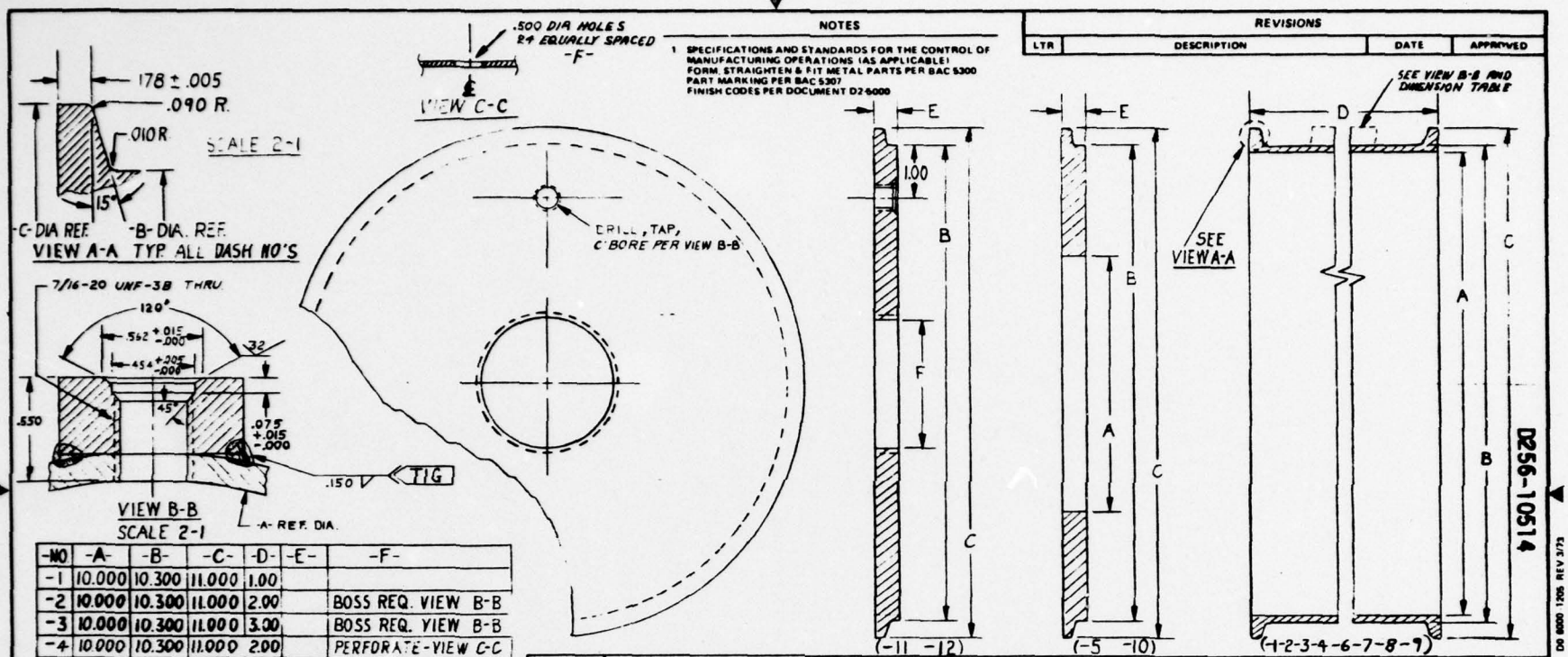

NOTES

1 SPECIFICATIONS AND STANDARDS FOR THE CONTROL OF MANUFACTURING OPERATIONS (AS APPLICABLE) FORM, STRAIGHTEN & FIT METAL PARTS PER BAC 5300
PART MARKING PER BAC 5307
FINISH CODES PER DOCUMENT D2-6000

REVISIONS

LTR	DESCRIPTION	DATE	APPROVED

-NO	-A-	-B-	-C-	-D-	-E-	-F-
-1	10.000	10.300	11.000	1.00		
-2	10.000	10.300	11.000	2.00		BOSS REQ. VIEW B-B
-3	10.000	10.300	11.000	3.00		BOSS REQ. VIEW B-B
-4	10.000	10.300	11.000	2.00		PERFORATE-VIEW C-C
-5	6.00	10.300	11.000		.500	
-6	8.000	8.300	9.000	1.00		
-7	8.000	8.300	9.000	2.00		BOSS REQ. VIEW B-B
-8	8.000	8.300	9.000	3.00		BOSS REQ. VIEW B-B
-9	8.000	8.300	9.000	2.00		PERFORATE VIEW C-C
-10	5.75	8.300	9.000		.500	
-11		10.300	11.000		.500	3.0-12 UNF -2B THD.
-12		8.300	9.000		.500	3.0-12 UNF -2 B THD.

PART NUMBER	NEXT ASSY	USED ON	EFFECTIVITY	REV LTR
		APPLICATION		

PART OR IDENTIFYING NUMBER	NOMENCLATURE OR DESCRIPTION	MATERIAL AND SPECIFICATION	HT TR	FINISH	PT MK	REV
-11 -12	FORWARD END PLATES	2024 T351 AL PLATE				
-5 -10	AFT END PLATES	2024 T351 AL PLATE				
-1-4-6-9	TUBE SECTIONS WITHOUT BOSS	6061 T6 AL PLATE OR TUBE OR 2024 T351				
-2-3-7-8	TUBE SECTIONS WITH BOSS	6061 T6 AL PLATE OR TUBE OR 2024 T351				

PARTS LIST

DIMENSIONING & TOLERANCING PER ANSI (USASI) Y 14.5
UNLESS OTHERWISE SPECIFIED
DIMENSIONS ARE IN INCHES
TOLERANCES: ANGLES ± 20'
DECIMALS .XX ± .030
DECIMALS .XXX ± .010
RIVET & BOLT EDGE MARG ± .05
BEND RADII ± .01 ON .03 & .06
± .03 ON .09 & GREATER
SHEET METAL CORNER RADII
INT .19 .16 EXT .25 .60

REVIEW & APPR: DWG QUAL | STRUCT | MATL & PRCS

CHANGE/ITEM NUMBER

CONTR
DWN A.B HUNTER 3/6/78
CHK
ENGR A.B HUNTER 3/27/78
ORG
PROJ

DWG ORIG BY (ORG)

THE BOEING COMPANY
CORPORATE OFFICES SEATTLE, WASHINGTON 98124

NOISE SUPRESSOR
END PLATES AND TUBE SECTIONS

SIZE	CODE IDENT NO	
B	81205	180-56693

SCALE 1/2 AS SHOWN

DRAWING RECORDS CLERK

D6 8000 1205 REV 3/73

A-8

A-9

NOTES

1 SPECIFICATIONS AND STANDARDS FOR THE CONTROL OF MANUFACTURING OPERATIONS (AS APPLICABLE)
FORM, STRAIGHTEN & FIT METAL PARTS PER BAC 5300
PART MARKING PER BAC 5307
FINISH CODES PER DOCUMENT D2-6000

REVISIONS

LTR	DESCRIPTION	DATE	APPROVED

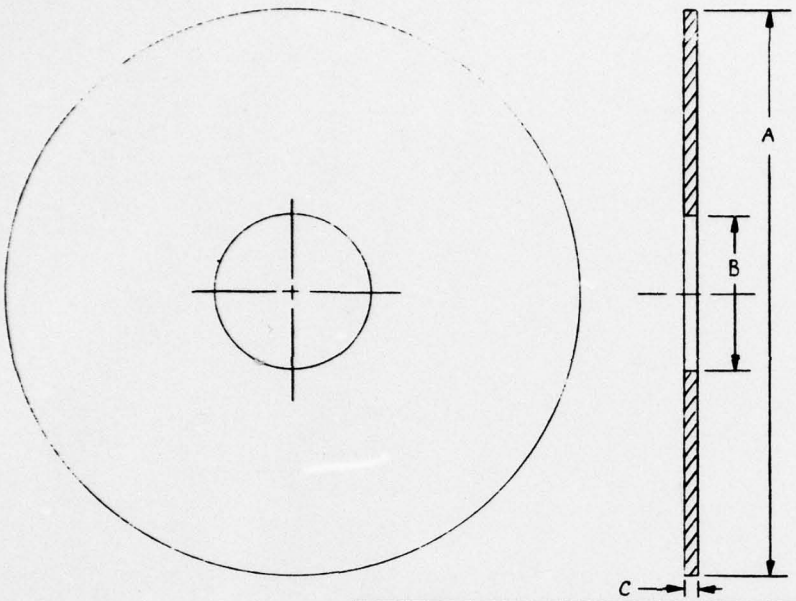

-NO.	-A-	-B-	-C-	
-1	11.000	2.55	.250	
-2	11.000	3.00	.250	
-3	11.000	4.00	.250	
-4	11.000	2.55	.063	
-5	9.000	2.55	.250	
-6	9.000	3.00	.250	
-7	9.000	4.00	.250	
-8	9.000	2.55	.063	
-9	11.000	10.00	.090	
-10	9.000	8.00	.090	

D256-10514

DD 6000 1205 REV 3/73

DRAWING RECORDS CLERK

PART OR IDENTIFYING NUMBER	NOMENCLATURE OR DESCRIPTION	MATERIAL AND SPECIFICATION	HT TR	FINISH	PT MK	REV
-4-8-9-10	BAFFLES & SPACERS	6061 T6 AL SHEET OR 2024 T3 AL.				
-1-2-3-5-6-7	BAFFLES	6061 T6 AL PLATE				

PARTS LIST

DIMENSIONING & TOLERANCING PER ANSI (USASI) Y 14.5
UNLESS OTHERWISE SPECIFIED
DIMENSIONS ARE IN INCHES
TOLERANCES: ANGLES ±
DECIMALS .XX ± .03
DECIMALS .XXX ± .010
RIVET & BOLT EDGE MARG ±.05
BEND RADII ± .01 ON .03 & .05
± .03 ON .09 & GREATER
SHEET METAL CORNER RADII
INT .19 .16 EXT .25 .00

REVIEW & APPR: DWG QUAL | STRUCT | MATL & PRCS

CONTR
DWN A.E. HUNTER 3/6/70
CHK
ENGR A.E. HUNTER 3/6/70
ORG
PROJ

THE BOEING COMPANY
CORPORATE OFFICES SEATTLE, WASHINGTON 98124

NOISE SUPRESSOR
BAFFLES

SIZE B | CODE IDENT NO 81205 | 180-56694
SCALE 1/2

PART NUMBER	NEXT ASSY	USED ON	EFFECTIVITY	REV LTR
		APPLICATION		

CHANGE/ITEM NUMBER

DWG ORIG BY (ORG)